Miner Deposita
DOI 10.1007/s00126-007-0150-6

ARTICLE

# New geologic, fluid inclusion and stable isotope studies on the controversial Igarapé Bahia Cu–Au deposit, Carajás Province, Brazil

**Ana M. Dreher · Roberto P. Xavier · Bruce E. Taylor · Sérgio L. Martini**

Received: 20 September 2005 / Accepted: 21 December 2006


**Abstract** The Igarapé Bahia Cu–Au deposit in the Carajás Province, Brazil, is hosted by steeply dipping metavolcano-sedimentary rocks of the Igarapé Bahia Group. This group consists of a low greenschist grade unit of the Archean (~2,750 Ma) Itacaiúnas Supergroup, in which other important Cu–Au and iron ore deposits of the Carajás region are also hosted. The orebody at Igarapé Bahia is a fragmental rock unit situated between chloritized basalt, with associated hyaloclastite, banded iron formation (BIF), and chert in the footwall and mainly coarse- to fine-grained turbidites in the hanging wall. The fragmental rock unit is a nearly concordant, 2 km long and 30–250 m thick orebody made up of heterolithic, usually matrix-supported rocks composed mainly of coarse basalt, BIF, and chert clasts derived from the footwall unit. Mineralization is confined to the fine-grained matrix and comprises disseminated to massive chalcopyrite accompanied by magnetite, gold, U- and light rare earth element (LREE)-minerals, and minor other sulfides like bornite, molybdenite, cobaltite, digenite, and pyrite. Gangue minerals include siderite, chlorite, amphibole, tourmaline, quartz, stilpnomelane, epidote, and apatite. A less important mineralization style at Igarapé Bahia is represented by late quartz–chalcopyrite–calcite veins that crosscut all rocks in the deposit area. Fluid inclusions trapped in a quartz cavity in the ore unit indicate that saline aqueous fluids (5 to 45 wt% NaCl+$CaCl_2$ equiv), together with carbonic ($CO_2$±$CH_4$) and low-salinity aqueous carbonic (6 wt% NaCl equiv) fluids, were involved in the mineralization process. Carbonates from the fragmental layer have $\delta^{13}C$ values from −6.7 to −13.4 per mil that indicate their origin from organic and possibly also from magmatic carbon. The $\delta^{34}S$ values for chalcopyrite range from −1.1 to 5.6 per mil with an outlier at −10.8 per mil, implying that most sulfur is magmatic or leached from magmatic rocks, whereas a limited contribution of reduced and oxydized sulfur is also evident. Oxygen isotopic ratios in magnetite, quartz, and siderite yield calculated temperatures of ~400°C and $\delta^{18}O$-enriched compositions (5 to 16.5 per mil) for the ore-forming fluids that suggest a magmatic input and/or an interaction with $^{18}O$-rich, probably sedimentary rocks. The late veins of the Igarapé Bahia deposit area were formed from saline aqueous fluids (2 to 60 wt% NaCl+$CaCl_2$ equiv) with $\delta^{18}O_{fluid}$ compositions around 0 per mil that indicate contribution from meteoric fluids. With respect to geological features, Igarapé Bahia bears similarity with syngenetic, volcanic-hosted massive sulfide (VHMS)-type deposits, as indicated by the volcano-sedimentary geological context, stratabound character, and association with submarine volcanic flows, hyaloclastite, and exhalative beds such as BIF and chert. On the other hand, the highly saline ore fluids and the

Editorial handling: S. Hagemann

A. M. Dreher (✉)
CPRM, Geological Survey of Brazil,
Av. Pasteur 404,
22290-240 Rio de Janeiro, RJ, Brazil
e-mail: amdreher@rj.cprm.gov.br

R. P. Xavier
Instituto de Geociências, UNICAMP,
Caixa Postal 6152,
13083-970 Campinas, SP, Brazil
e-mail: xavier@ige.unicmap.br

B. E. Taylor
Geological Survey of Canada,
601 Booth Street,
Ottawa, ON K1A 0E8, Canada
e-mail: betaylor@nrcan.gc.ca

S. L. Martini
Metaldom Ltda.,
Rua Osório de Almeida 15/201,
22291-000 Rio de Janeiro, RJ, Brazil
e-mail: martini.s@uol.com.br

mineral assemblage, dominated by magnetite and chalcopyrite, with associated gold, U- and LREE-minerals and scarce pyrite, indicate that Igarapé Bahia belongs to the Fe oxide Cu–Au (IOCG) group of deposits. The available geochronologic data used to attest syngenetic or epigenetic origins for the mineralization are either imprecise or may not represent the main mineralization episode but a later, superimposed event. The C, S, and O isotopic results obtained in this study do not clearly discriminate between fluid sources. However, recent B isotope data obtained on tourmaline from the matrix of the fragmental rock ore unit (Xavier, Wiedenbeck, Dreher, Rhede, Monteiro, Araújo, *Chemical and boron isotopic composition of tourmaline from Archean and Paleoproterozoic Cu–Au deposits in the Carajás Mineral Province*, 1° Simpósio Brasileiro de Metalogenia, Gramado, Brazil, extended abstracts, CD-ROM, 2005) provide strong evidence of the involvement of a marine evaporitic source in the hydrothermal system of Igarapé Bahia. Evaporite-derived fluids may explain the high salinities and the low reduced sulfur mineral paragenesis observed in the deposit. Evaporite-derived fluids also exclude a significant participation of magmatic or mantle-derived fluids, reinforcing the role of nonmagmatic brines in the genesis of Igarapé Bahia. Considering this aspect and the geological features, the possibility that the deposit was generated by a hydrothermal submarine system whose elevated salinity was acquired by leaching of ancient evaporite beds should be evaluated.

**Keywords** Igarapé Bahia · Carajás Mineral Province · Iron oxide (Cu–Au) · Brazil

## Introduction

The Igarapé Bahia deposit contains estimated reserves of 219 Mt at 1.4% Cu and 0.8 g/t Au (Tallarico et al. 2005) and belongs, with the Salobo, Sossego, and Cristalino deposits, to the group of large-tonnage Cu–Au deposits of the Carajás Mineral Province in northern Brazil. Similarly to the other deposits, Igarapé Bahia is also hosted by late Archean (~2,750 Ma) metavolcano-sedimentary rocks of the Itacaiúnas Supergroup, contains a mineral assemblage dominated by chalcopyrite and magnetite with associated gold and U- and light rare earth element (LREE)-minerals, and was formed from highly saline mineralizing fluids.

The metal association and the hypersaline fluids have led many researchers; (e.g., Huhn and Nascimento 1997; Tazava and Oliveira 2000; Ronzé et al. 2000; Santos 2002; Laux et al. 2003) to include Igarapé Bahia in the Fe oxide Cu–Au (IOCG) class of deposits, as defined by Hitzman et al. (1992), and to admit that the deposit is epigenetic and related to granitic magmatism. Sensitive high resolution ion microprobe (SHRIMP II) U–Pb dating at 2,575±12 Ma obtained by Tallarico et al. (2005) on ore-related monazite of Igarapé Bahia appears to corroborate the epigenetic nature of mineralization as well as its link with coeval granites that occur in the Carajás region.

Another group of authors (e.g., Ferreira Filho 1985; Almada and Villas 1999; Villas and Santos 2001; Dreher 2004) have chosen the volcano-sedimentary geological context as the prime criterion to attribute a syngenetic origin for Igarapé Bahia. Lead-Pb isotope data on chalcopyrite yielded ages around 2,750 Ma (from 2,754±36 to 2,777±22 Ma, Galarza 2002; Galarza et al. 2006), similar to the deposit host rocks. However, these sulfide Pb–Pb ages are considered, in general, as nonrobust age dates so that the contemporaneity between mineralization and host rock sequence remains undemonstrated.

This notwithstanding, recent geologic, fluid inclusion and stable isotope data, albeit not definitive of a syngenetic origin, raise interesting aspects such as that the age of the main mineralization event may be older than the 2,575 Ma age obtained by Tallarico et al. (2005), that more than one mineralization episode may have occurred at the deposit site, and that mineralization may not have had a significant link to granitic magmatism but instead to evaporite-derived fluids.

The present article describes briefly the regional and local geology of the Igarapé Bahia deposit, followed by new geologic and petrographic observations from drill core, and by fluid inclusion and stable isotope studies. A discussion on the genesis of the deposit is then presented to point out the main aspects or causes of controversy.

## Regional geology

The Carajás Mineral Province is one of the most important mineral districts of Brazil, comprising an extensive area in the eastern part of the Amazonian Craton (Fig. 1). The oldest geological unit of the region is a gneiss–migmatite basement known as Xingu Complex, which was metamorphosed at ca. 2,850 Ma (Machado et al. 1991). In the northern part of the province (Fig. 1), the Xingu Complex is overlain by metavolcano-sedimentary sequences of the Itacaiúnas Supergroup, about 2,750 Ma in age (Machado et al. 1991; Trendall et al. 1998), which is in turn covered by a metasedimentary unit named Águas Claras Formation, deposited between 2,750 and 2,650 Ma (Dias et al. 1996).

The volcanic and sedimentary rocks of the Itacaiúnas Supergroup underwent metamorphism from lower greenschist to upper amphibolite facies. Most researchers (e.g., Gibbs et al. 1986; Docegeo 1988; Olszewski et al. 1989; Lindenmayer and Fyfe 1992; Winter 1994; Villas and Santos 2001) believe the Itacaiúnas rocks were generated and deposited in an ensialic rift environment, although others (Dardenne et al. 1988; Teixeira and Eggler 1994)

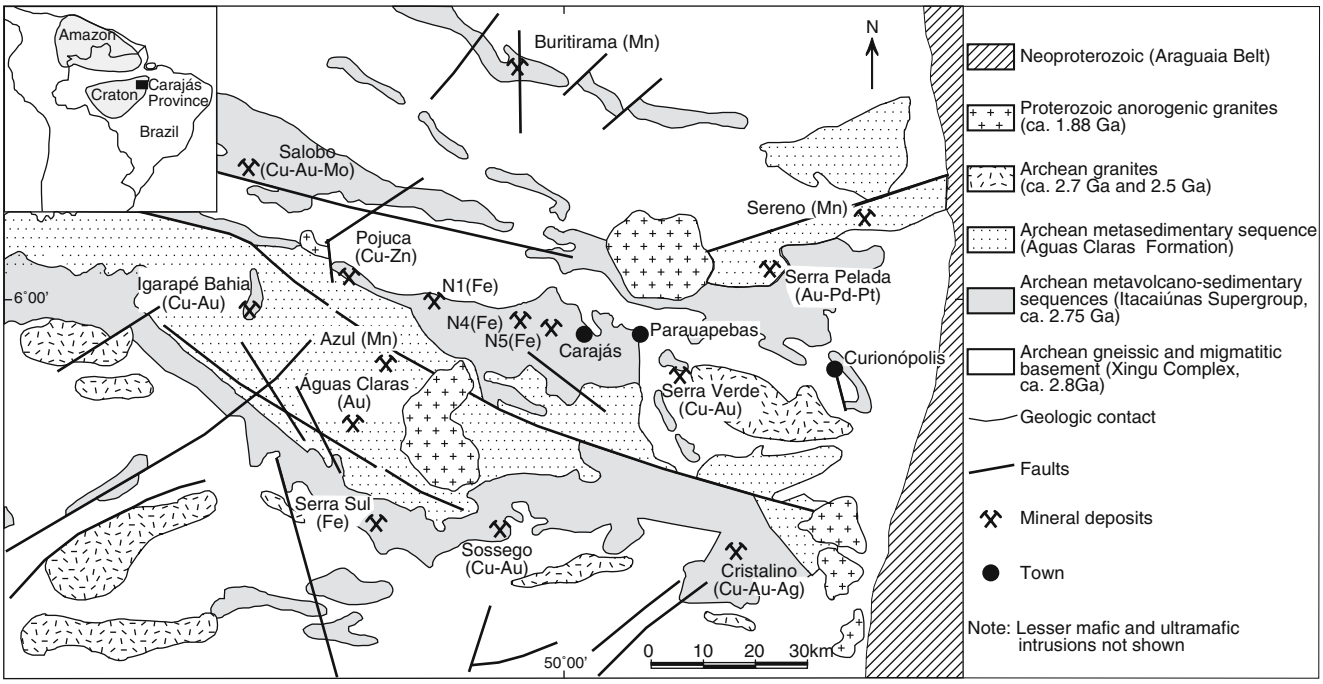


**Fig. 1** Geological map of the northern part of the Carajás Mineral Province, Brazil, showing the location of the Igarapé Bahia and other important Cu–Au, Fe and Mn deposits (based on Docegeo 1988)

propose they formed in a subduction-related setting. The Águas Claras Formation is metamorphosed to lower greenschist facies and is composed mainly of arenites of shallow-marine and fluvial settings.

The Itacaiúnas Supergroup hosts, besides Igarapé Bahia, other important mineral deposits of the Carajás Province, namely, the magnetite–Cu–Au deposits of Salobo, Sossego, and Cristalino, the Pojuca Cu–Zn deposit, the large banded iron formations known mainly near the town of Carajás (e.g., N1, N4, and N5), and the manganese deposits of Sereno and Buritirama (Fig. 1).

Deformed granites dated at ca. 2,750 and 2,570 Ma (Barros et al. 2004; Machado et al. 1991), minor late-Archean mafic sills and dikes, and undeformed, anorogenic granites of 1,880 Ma (Tallarico et al. 2004) intrude the older metamorphic units.

## Local geology

The Igarapé Bahia Cu–Au deposit lies 70 km west of the town of Carajás in an area dominated by metasedimentary rocks of the Águas Claras Formation (Fig. 1). The deposit occurs in a small erosional window and is hosted by rocks of the Igarapé Bahia Group, which is considered as a low greenschist-grade unit of the Archean (~2,750 Ma) metavolcano-sedimentary Itacaiúnas Supergroup (Docegeo 1988). The upper part of the deposit is made up of a 100 to 150-m thick gossan–laterite zone from which significant amounts of gold were mined until 1992 by Companhia Vale do Rio Doce (CVRD). The lower part of the deposit contains hypogene Cu–Au mineralization, hosted by a hydrothermally altered fragmental rock unit situated between a footwall mainly composed of mafic metavolcanic rocks and a dominantly metasedimentary hanging-wall sequence.

The fragmental unit is a steeply dipping, roughly tabular and concordant orebody that has gradational contacts with its wallrocks. It is about 2 km long and 30 to 250 m thick and is disrupted by various faults and mafic dikes (Fig. 2). The three main segments of the mineralized unit, known as Acampamento Norte (ACN), Acampamento Sul (ACS), and Furo Trinta (F30) orebodies, dip steeply (about 80° NW, NE, and SE, respectively) conforming to a semicircular feature, as shown in Fig. 2. The so-called Alemão deposit (Barreira et al. 1999; Ronzé et al. 2000), situated immediately northwest of Igarapé Bahia below a cover of Águas Claras meta-arenites (Fig. 2), represents a particularly magnetite–Cu–Au-enriched down-faulted segment of the ACN orebody. Resources for Alemão have been quoted as 170 Mt at 1.5% Cu and 0.8 g/t Au (Cordeiro 1999). According to Santos (2002), the Alemão segment consists of a concordant, almost vertically dipping, mineralized fragmental rock body, about 500 m long and up to 250 m thick (Fig. 3a). At the ACS orebody, the fragmental layer is about 50–100 m in thickness and wedges out to about 30 m at the F30 orebody (Fig. 3b–d).

Mineralization is concentrated in the matrix of the fragmental rock and consists of disseminated to locally massive, fine-grained chalcopyrite with associated magnetite, gold, U- and LREE-minerals, and minor other sulfides

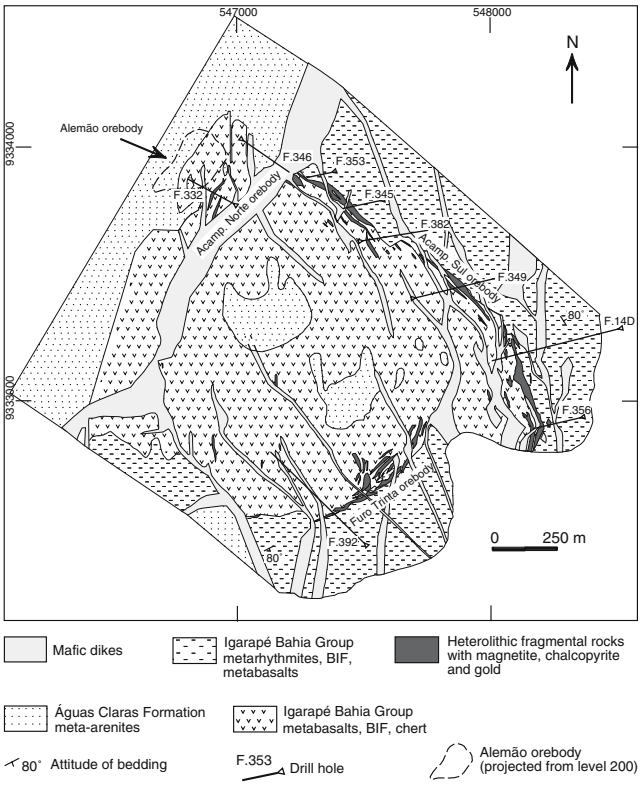


**Fig. 2** Geological map of the Igarapé Bahia mine and location of the investigated drill-holes (slightly modified from CVRD, 2000, Mapa geológico escala 1:12.500 de Igarapé Bahia e secções verticais, unpublished)

like cobaltite, bornite, molybdenite, digenite, and pyrite. Fine-grained chalcopyrite also occurs as disseminations in some brecciated footwall metabasalts as well as in nodules and pore-space fillings in the upper metasedimentary rocks. Chalcopyrite is also present in tabular, centimeter-thick, coarse-grained quartz–carbonate–sulfide veins that crosscut the fragmental unit, the hosting metavolcanic and metasedimentary rocks, and the younger Águas Claras metaarenites and some of the mafic dikes as well.

U–Pb dating of zircons from the footwall metavolcanic rocks of Igarapé Bahia yielded a SHRIMP II age of 2,748±34 Ma (Tallarico et al. 2005) and a Pb evaporation age of 2,745±1 Ma (Galarza and Macambira 2002; Galarza 2002). These ages correlate well with the Itacaiúnas metabasaltic rocks, which have a U–Pb zircon age of 2,759±2 Ma (Machado et al. 1991). The unmetamorphosed mafic dikes that crosscut the metavolcano-sedimentary rocks, the ore unit, as well as the Águas Claras metasedimentary rocks (Fig. 2) have a maximum SHRIMP II age on zircon xenocrysts of ca. 2,670 Ma (between 2,691±52 and 2,653±48 Ma, Tallarico et al. 2005).

Contrasting ages have been obtained for the Igarapé Bahia mineralization. Lead-Pb isotope data on chalcopyrite and gold give ages around 2,750 Ma (2,777±46 Ma and 2,744±12 Ma) for the Igarapé Bahia orebodies (Galarza 2002; Galarza et al. 2006) and around 2,550 Ma (from 2,521±56 to 2,595±200 Ma) for the Alemão orebody (Santos 2002). A SHRIMP II U–Pb age of 2,575±12 was obtained by Tallarico et al. (2005) on hydrothermal monazite from the matrix of the ore-bearing magnetite–breccias of Igarapé Bahia.

## Materials and methods

The study of the Igarapé Bahia rocks involved detailed examination of nine regularly spaced drill holes that transect the different orebodies of the deposit (see Fig. 2). Ninety polished thin sections were studied microscopically.

Microthermometric, Raman microspectroscopy, and scanning electron microscope analyses of fluid inclusions were

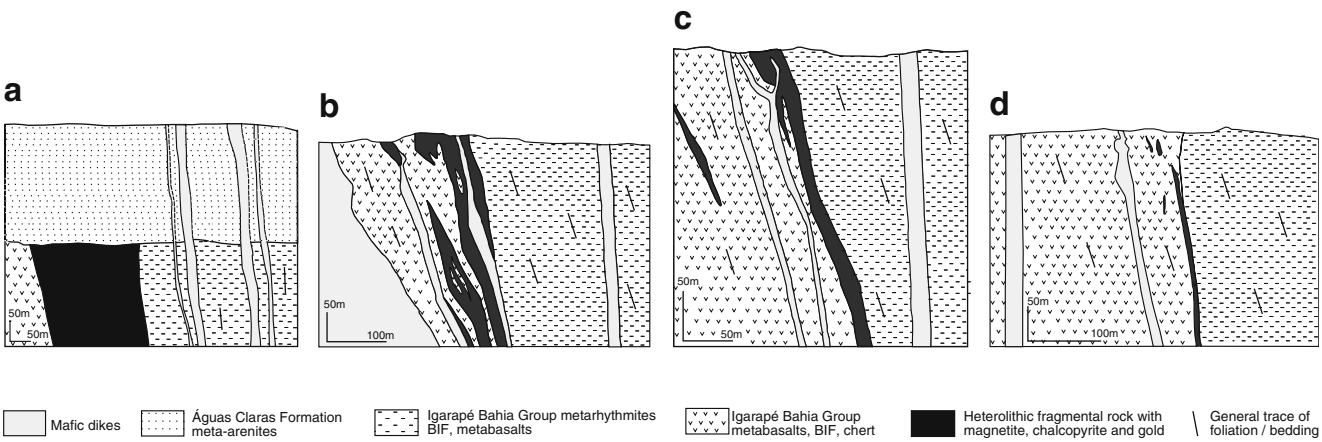


**Fig. 3** Vertical sections of the Igarapé Bahia Cu–Au deposit. **a** Alemão orebody (extracted from Santos 2002). **b** and **c** Acampamento Norte orebody (slightly modified from CVRD, 2000, Mapa geológico escala 1:12.500 de Igarapé Bahia e secções verticais, unpublished). **d** Furo Trinta orebody (slightly modified from CVRD, 2000, Mapa geológico escala 1:12.500 de Igarapé Bahia e secções verticais, unpublished)

performed at the Instituto de Geociências, University of Campinas, Brazil, on six doubly polished plates of quartz. Microthermometry measurements of inclusion fluids were performed on a LINKAM THMSG600 stage attached to a conventional petrographic microscope. The stage was calibrated using synthetic fluid inclusions to a precision of ±0.3°C for freezing runs down to −56.6° and to ±3°C for heating runs up to 500°C. Laser Raman microspectroscopy analyses of non-aqueous phases in selected individual fluid inclusions were obtained by means of a T64000 Jobin Yvon spectrometer coupled with a CCD detector cooled with liquid $N_2$. Irradiation was by the 514.5-nm line of an argon laser, with an output of 600 mW laser power at the source. An energy dispersive spectroscopy (EDS)-equipped electron microscope, model LEO 430i, was used in the identification of solid phases contained in opened fluid inclusions.

Stable isotope analyses of C, O, and S were carried out on 68 samples from the Igarapé Bahia deposit. Fine-grained, siderite-rich whole-rock samples of the ore unit were powdered and analyzed. Coarse-grained vein quartz, carbonate, chalcopyrite, and magnetite were separated by hand-picking. Fine-grained magnetite and chalcopyrite from the ore unit were separated by using a hand magnet and nonmagnetic tweezers, respectively. Carbonate samples were first submitted to X-ray diffraction at the Instituto de Geociências, University of São Paulo, for identification of the carbonate species. The C and O isotopic ratios were obtained at the Laboratório de Ecologia Isotópica, Centro de Energia Nuclear na Agricultura (CENA), in Piracicaba, São Paulo, involving extraction methods described in McCrea (1950) and Al-Assam et al. (1990) and analyses performed on a VG Micromass 602 spectrometer. The O and S isotope analyses on quartz, magnetite, and chalcopyrite were carried out at the Light Stable Isotope Laboratory of the Geological Survey of Canada, in Ottawa. Extraction of O isotopes followed conventional methods developed by Clayton and Mayeda (1963). Sulfur isotopes in chalcopyrite were analyzed using the micro-isotopic laser extraction system (MILES) technique (Taylor and Beaudoin 1993; Beaudoin and Taylor 1994). Analyses were performed on a Finnigan MAT 252 spectrometer.

## The host rocks of the Igarapé Bahia deposit

### Footwall rocks

The footwall rocks to the mineralized fragmental unit of Igarapé Bahia are mainly metabasalts with associated quartz–magnetite banded iron formation (BIF), chert, diabase, and minor clastic sedimentary rocks. The metabasalts constitute fine-grained, strongly chloritized, meter-thick flows displaying massive, fine amygdaloidal or brecciated structures. A slight foliation is visible in places. The brecciated basalts are interbedded with the massive and amygdaloidal types and can be, in most cases, characterized as in situ hyaloclastite and autobreccia, formed of aphanitic, probably vitric, particles arranged in a jigsaw-fit texture (Fig. 4a). Autobreccia and hyaloclastite are considered as non-explosive volcanic products formed by quench fragmentation of lavas in contact with cold seawater (McPhie et al. 1993). Pillow structures could not be recognized in drill core and pyroclastic rocks, as those mentioned by Tallarico et al. (2005), were not identified in this unit. The BIF and chert layers amidst the mafic flows indicate hiatuses in volcanism that were appropriate for chemical precipitation from submarine hydrothermal vents. Banded oxide–silicate iron formations are in fact widespread throughout the Carajás region, typically associated with the mafic volcanic rocks of the Itacaiúnas Supergroup.

### Mineralized fragmental rocks

The mineralized fragmental rocks are heterolithic, mostly matrix-supported rocks, containing coarse lithic clasts set in a fine-grained, massive to foliated matrix. The clasts are mainly of basalt and quartz–magnetite BIF derived from the footwall unit (Fig. 4b–d). Lesser chert, siliciclastic sedimentary rock, and brecciated BIF fragments are also present. The clasts are poorly sorted, ranging from millimeters to more than a meter in length and displaying angular to rounded borders. Jigsaw-fit textures are rare in these rocks, and no layering is visible, although locally some clasts may be oriented and aligned.

The fine-grained matrix is formed mainly of hydrothermal phases like magnetite, chalcopyrite, chlorite, and carbonate, with variable amounts of amphibole, quartz, stilpnomelane, epidote, apatite, tourmaline, pyrosmalite, and a large variety of accessory minerals containing elements such as Mo, Co, W, F, P, Mn, Sn, Ag, Cl, U, and LREE. Other minerals such as grunerite, cummingtonite, talc, pyrrhotite, sphalerite, and galena are described from the Alemão segment (Santos 2002). At Alemão and its adjacent ACN and northern ACS orebodies, the most common minerals are Fe-rich phases like magnetite, chalcopyrite, siderite, chamosite, stilpnomelane, and amphibole. A temperature of ~400°C is estimated for the assemblage Fe–actinolite–hastingsite–stilpnomelane–magnetite observed in this part of the deposit (Dreher 2004), based on parageneses that occur in low-grade metamorphosed oxide–silicate iron formations (Klein 1973). In less mineralized zones, as in the southern ACS and F30 orebodies, hydrothermal alteration is dominated by chlorite. Exceptionally matrix-rich fragmental rocks with diffuse banding and containing scattered, apparently corroded and partly replaced clasts also occur, particularly in stratigraphically lower levels of the Alemão and neighboring orebodies. These rocks have

been termed hydrothermalites by various authors (Ronzé et al. 2000; Tazava and Oliveira 2000) and are made up of almost pure chalcopyrite and magnetite.

According to Tallarico et al. (2005), the fragmental rocks are rich in Ba, F, P, containing up to 15 g/t Au, 380 ppm U, and La and Ce contents of up to 1,000 ppm each. Gold is more commonly associated with sulfides like cobaltite and chalcopyrite but may also be found as inclusions in other minerals (Daleffe 2001). Magnetite is normally subhedral or anhedral (Fig. 4e), but euhedral grains are also present. Siderite is late in the paragenesis compared to magnetite and to the silicates. Chalcopyrite is invariably anhedral, suggesting that it crystallized later than all other phases.

Most fragmental rocks are slighty foliated and contain elongate chalcopyrite grains (Fig. 4c–g) suggesting that they were submitted to the same lower greenschist-grade metamorphism that affected the Igarapé Bahia Group wallrocks. The lithic clasts are in many cases foliated parallel to the matrix. This internal fabric can be observed in basalt, in chlorite-bearing chert, and in siliciclastic rock fragments (Fig. 4f,g). However, no foliation is visible in the BIF (Fig. 4h) or in pure chert clasts, which invariably show fine granoblastic textures. Strongly foliated fragmental rock specimens from the Alemão orebody are described and illustrated by Ronzé et al. (2000) and Santos (2002).

## Hanging wall rocks

The rocks that overlie the fragmental unit are mainly clastic metasedimentary rocks such as arenites, siltites, and argillites. Less common rocks include BIF, chert, and metabasalt. The clastic rocks have been termed rhythmites by Docegeo (1988) and are, in this paper, interpreted as a turbiditic assemblage.

Arenites are dominant in the lower part of the hanging wall sequence. They constitute either centimeter-thick, fining upward units that grade into siltite and argillite or massive, up to meter-thick beds with poor or inexistent particle size grading and lacking internal stratification. These arenites were possibly deposited from high-density turbidity flows. Laminated siltite–argillite strata occur more commonly towards the middle and upper parts of the hanging wall pile, although in the northern ACS orebody, they lie directly on top of the fragmental layer. These rocks are commonly interpreted as distal D–E turbidites (Bouma 1962), deposited from medium to low density currents. In general, the clastic metasedimentary rocks are slightly foliated and composed mainly of chlorite, sericite, angular to subrounded quartz grains, and lesser feldspar and biotite. Chert, mafic to felsic volcanic particles and argillite rip-up clasts occur in the arenites. Juvenile pyroclasts, such as the pumice fragments described by Ferreira Filho (1985), were not recognized, implying that the hanging wall rocks are essentially detrital sedimentary deposits rather than syn-eruptive products.

**Fig. 4** The Igarapé Bahia deposit rocks. **a** Footwall hyaloclastite showing a brecciated texture. Fragments are not well defined on the left half of the sample, but angular clasts can be seen on the right side, displaying a jigsaw-fit texture characteristic of quench fragmentation. Sample F382/162.30 m. **b** Heterolithic, matrix-supported fragmental rock containing large angular BIF clasts and smaller, rounded, chert particles set in a fine-grained matrix. Sample F392/340.60 m. **c** Matrix-supported fragmental rock containing a large BIF clast set in a fine-grained, slightly foliated matrix made up of Fe-rich silicates, magnetite, and chalcopyrite. Sample F353/166.75 m. **d** Fragmental rock formed of large, rounded, massive-textured metabasalt clasts (*mb*) surrounded by a slightly foliated, siderite–chalcopyrite matrix. Sample F382/241.00 m. **e** Photomicrograph of the matrix of a fragmental rock sample showing elongate chalcopyrite (*ccp*) and anhedral magnetite (*mag*). Sample F382/242.10 m. Reflected light. **f** Photomicrograph of a fragmental rock containing internally foliated chloritic chert particles set in a foliated matrix made up of chlorite, carbonate, and disseminated, elongate, chalcopyrite grains (in *black*). Sample F382/287.15 m. Plane polarized light. **g** Fragmental rock composed of siliciclastic rock fragments set in a fine-grained, strongly foliated matrix. The siliciclastic rock fragments are foliated parallel to the foliation of the matrix. Sample F345/184.00 m. Plane polarized light **h** Fragmental rock composed of nonfoliated quartz–magnetite BIF clasts set in a strongly foliated, chlorite-rich matrix. Sample F332/265.80 m. **i** Hanging-wall argillite–siltite–metaturbidites, showing contorted bedding caused by folding and small-scale faulting. Samples F353. **j** Disrupted bedding in hanging-wall metasedimentary rock. Disruption was probably caused by fault-related synsedimentary slump and dewatering processes. Sample F392/248.30 m

Striking features of these upper metasedimentary rocks are their abundant slide, slump, and disruption structures as well as the presence of breccia and conglomerate interbeds. These features occur in between apparently undeformed layers, suggesting that they formed mostly in situ and are related to repeated tectonic disturbances probably linked to growth faulting. The fine laminated turbidites commonly display contorted bedding caused by folds or small-scale faults (Fig. 4i), which may indicate partial lithification by the time of deformation. The coarser-grained arenite–turbidites, in turn, frequently show bedding disruption (Fig. 4j), possibly associated with liquefaction or fluidization processes (Lowe 1975), whereas breccia and conglomerate interbeds record yet more advanced deformation, involving disaggregation and even reworking of locally-derived sediments.

## The Águas Claras meta-arenites

The rocks of the Águas Claras Formation that cover part of the Alemão and also the ACN orebodies of Igarapé Bahia are greyish green, slightly foliated and more or less chloritized and silicified arenites. They are composed dominantly of rounded to subrounded, coarse sand- to granule-sized quartz grains, with lesser chert, feldspar, and volcanic rock particles. Chlorite and sericite are the main components of the matrix, where accessory minerals like tourmaline, rutile, and rounded zircon grains also occur. A powdery black, probably carbonaceous, substance is also locally found in the matrix.

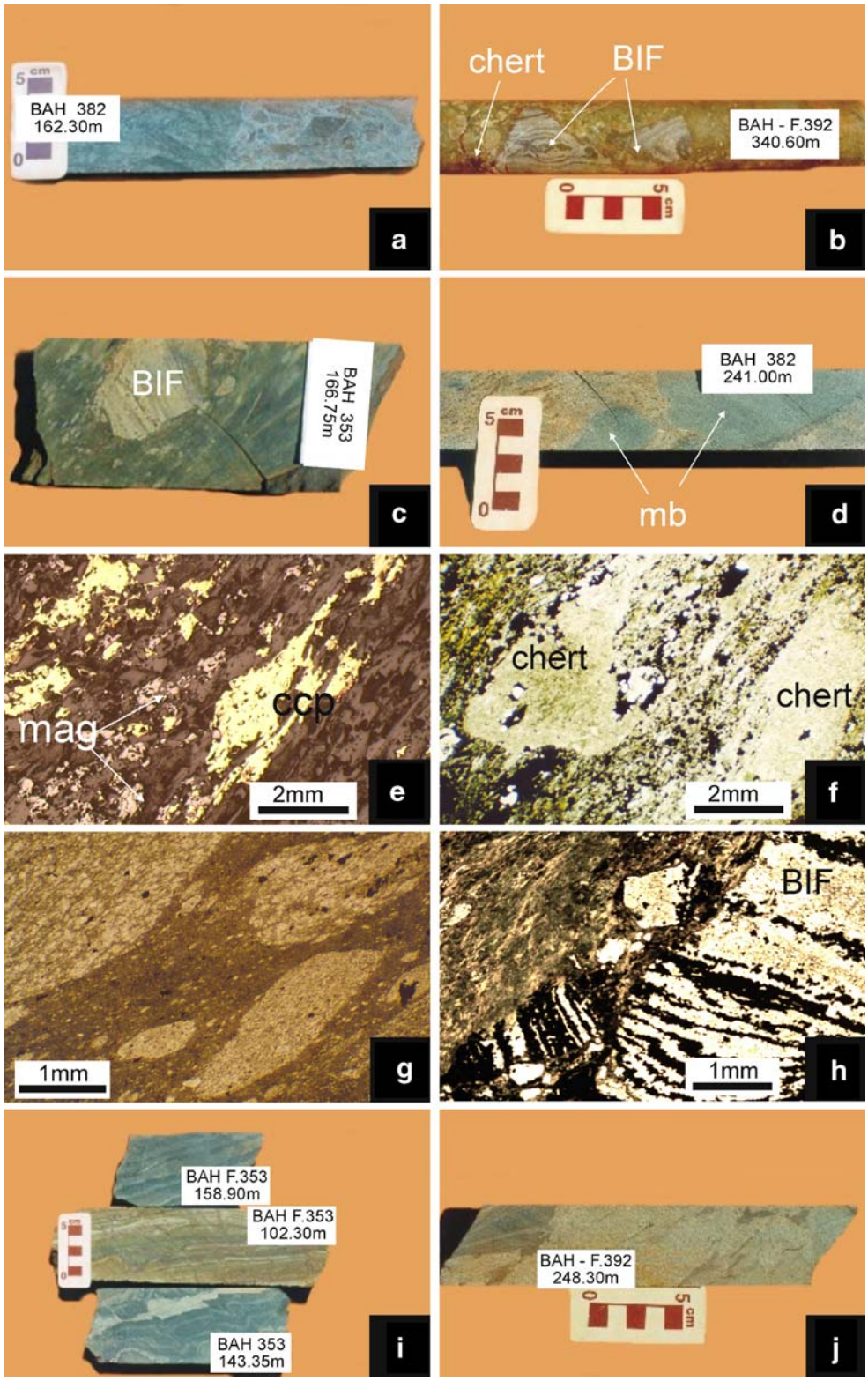


Mafic dikes

The many mafic dikes that transect the Igarapé Bahia deposit area are nonfoliated rocks, of basaltic to dioritic composition, that usually display subophitic textures. They vary from unaltered to chlorite–sericite–biotite-altered rocks but are not mineralized. An alteration border of chlorite, carbonate, epidote, and reddish feldspar is observed at the contact with crosscutting quartz–calcite–chalcopyrite veins. The mafic dikes in the Igarapé Bahia

area have a roughly N–S orientation (Fig. 2), and most of them extend for several kilometers cutting the Águas Claras unit. Other similar dikes in the Carajás region follow this same N–S trend.

Late veins

Several chalcopyrite-bearing veins occur in the Igarapé Bahia deposit area. These veins crosscut all rock types, including the fragmental layer and some of the mafic dikes, and therefore appear to represent late, low-grade mineralizing events at Igarapé Bahia. The veins are mostly planar and narrow (1 to 4 cm thick) and may display brecciated borders. Differently from the fragmental rocks, which are formed of fine-grained magnetite, chalcopyrite, siderite and Fe–chlorite, the veins are dominantly composed of unstrained, coarse-grained, commonly comb-textured quartz, plus calcite and chalcopyrite (Fig. 5d). Minor pyrite, chlorite, K-feldspar, siderite, specular hematite, and magnetite are also present.

## Fluid inclusion study

Sample selection, petrography and inclusion types

Samples for the fluid inclusion study were selected from quartz of a cavity contained in the mineralized fragmental unit and from quartz of five veins that crosscut the Igarapé Bahia deposit rocks.

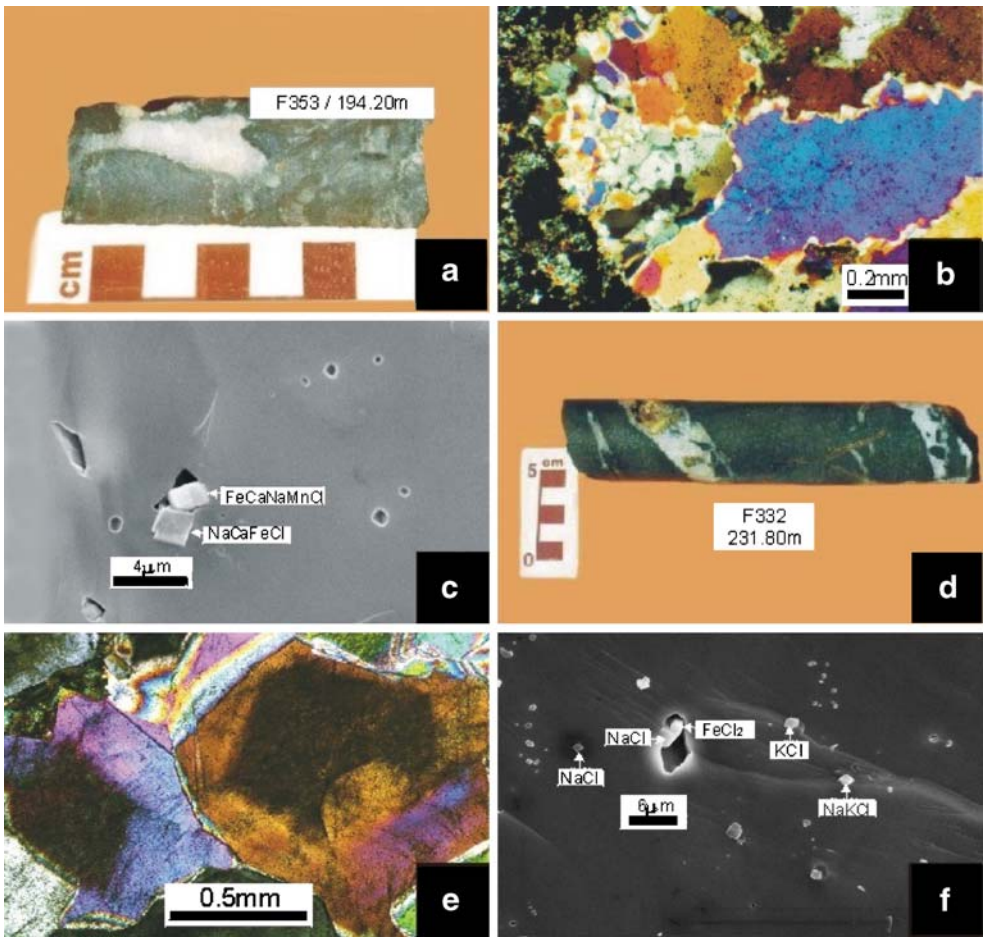


**Fig. 5** Macroscopic and microscopic features of samples selected for fluid inclusion studies. **a** Quartz cavity in mineralized fragmental rock. The fragmental rock contains small BIF clasts set in a fine-grained matrix made up of chalcopyrite, magnetite, fibrous amphibole, and carbonate. Sample F353/194.20 m. **b** Photomicrograph of the quartz cavity showing large quartz crystals containing abundant fluid inclusions, interpreted as primary and pseudo-secondary. The fine-grained, recrystallyzed quartz aggregates situated between the larger crystals are almost devoid of inclusions. Sample F353/194.20 m. Cross-polarized light. **c** Scanning electron microscope image showing complex Fe–Mn–Na–Ca–Cl solids in opened fluid inclusion cavities. Sample F353/194.20 m. **d** Typical narrow, brecciated quartz–chalcopyrite–calcite veins cutting a meta-arenite of the Águas Claras Formation. Sample F382/231.80 m. **e** Photomicrograph showing idiomorphic vein-quartz crystals containing primary growth-zone fluid inclusions. Sample F382/231.80 m. **f** Scanning electron microscope image showing halite (NaCl), Fe–chloride ($FeCl_2$) and sylvite (KCl) daughter crystals in and around opened fluid inclusion cavities. Sample F332/286.45 m

The cavity quartz provides one of the few samples of coarse-grained and relatively pure quartz found in the ore unit. This quartz is considered to preserve the record of fluids responsible for the hydrothermal event that mineralized the fragmental rock unit. The studied sample (Fig. 5a) comes from drill hole F353 that intersects the northern ACS orebody. The cavity is occupied by quartz crystals of 0.1 to 4 mm in length. Quartz crystals are strained and have fine mosaic-recrystallized borders due to metamorphism but preserve a drusy concentric arrangement typical of open-space fillings (Fig. 5b). Minerals like magnetite, fibrous amphibole, siderite, and chalcopyrite that occur in the host ore unit are also present in the cavity as minute grains included in, or situated between, the quartz crystals.

The veins that crosscut all rocks in the deposit area are believed to represent late, low-grade mineralizing events at Igarapé Bahia. Samples for the fluid inclusion study include quartz from veins that cut the ACS orebody (F382), the Águas Claras metasedimentary rocks that recover the ACN orebody (F332; Fig. 5d), and quartz from a vein that transects a mafic dike (F375). Quartz crystals in the veins contrast with the cavity quartz by being unstrained, subhedral to euhedral in shape, and commonly displaying growth zones (Fig. 5e).

Three main types of fluid inclusions were distinguished in all the selected samples, on the basis of phases present at room temperature:

Type 1 These correspond to aqueous, two-phase liquid–vapor inclusions, in which the vapor bubble represents 5–10% of the inclusion volume.

Type 2 These inclusions are multiphase, saline-aqueous inclusions, which are divided into a 2A subtype, characterized by the presence of one or two solid phases and a vapor bubble that together make up 25 vol.% of the inclusion; and a 2B subtype, in which more than two solids and a vapor phase fill together around 40% of the cavity volume.

Type 3 These are $CO_2$-bearing inclusions, divided into a 3A aqueous-carbonic subtype, made up of water, liquid and gaseous $CO_2$, in which the carbonic phases occupy 20 up to 90 vol.% of the inclusions; and a 3B carbonic subtype, which is totally occupied by liquid $CO_2$ or liquid plus gaseous $CO_2$. The type 3, $CO_2$-bearing inclusions are normally darker and larger than types 1 and 2 aqueous inclusions.

## Microthermometry

During microthermometric experiments, most of the aqueous type 1 and type 2 inclusions froze at temperatures between −70° and −90°C. Upon heating, first melting (Te) and ice-melting temperatures ($Tm_{ice}$) were registered for the majority of the aqueous inclusions, whereas only a few hydrohalite melting temperatures ($Tm_{HH}$) were recorded due to the metastability behavior of this phase. Type 1 inclusions always homogenized to the liquid phase ($Th_{(LV-L)}$), whereas type 2 inclusions homogenized by the dissolution of halite ($Tm_H$) after the disappearance of vapor to the liquid ($Th_{(SLV-SL)}$). The salinities of the aqueous inclusions, in terms of weight percent NaCl equivalent (wt% NaCl equiv), were estimated for the type 1 inclusions from $Tm_{ice}$ values and the equation of Bodnar (1993), whereas for the type 2 inclusions from the $Tm_H$ values and the equation of Sterner et al. (1988). Additionally, the bulk composition of these inclusions were determined graphically from $Tm_{ice}$, $Tm_{HH}$, and $Tm_H$ in the ternary NaCl–$CaCl_2$–$H_2O$ diagram, following the method of Williams-Jones and Samson (1990), and given in terms of total salts (wt% NaCl+$CaCl_2$ equiv).

Type 3 inclusions underwent freezing around −100°C. On warming, the temperatures of $CO_2$ melting ($Tm_{CO2}$) and homogenization to the liquid phase ($Th_{CO2(L)}$) were recorded. The $CO_2$ densities were obtained graphically from the homogenization curve of Shepherd et al. (1985). The few melting temperatures of clathrate ($Tm_C$) for subtype 3A inclusions were used to calculate salinity values on the basis of the equation of Chen (1972). Total homogenization temperatures were not registered because all type 3 inclusions leaked or decrepitated on heating to temperatures above 250°–300°C.

## Results from the quartz cavity sample

A summary of the microthermometric data of fluid inclusions studied in the quartz cavity are given in Table 1. Large clusters or within-grain planar arrays containing inclusion types 1, 2, and 3 ranging from 4 to 10 μm in diameter are dominant in nonrecrystallized quartz grains of this sample (Fig. 5b). Following the criteria of Roedder (1984), the fluid inclusion assemblages in clusters and planar arrays are interpreted as of possible primary and pseudo-secondary origin, respectively. Within the clusters or planar arrays, the aqueous inclusions (types 1 and 2) occur in approximately the same amount as the $CO_2$-bearing (type 3) inclusions. Additionally, subtype 2A inclusions are abundant compared to rare 2B inclusions. The common coexistence of inclusion types 1, 2, and 3 in single clusters or planar arrays strongly suggests that these inclusions may have undergone coeval trapping during quartz precipitation.

Types 1 and 2 aqueous inclusions of the quartz cavity present Te that range from −43° to −72°C and $Tm_{ice}$ that vary widely from −3° to −47°C (Fig. 6a,b), indicating that the trapped fluids contain a complex mixture of metal chlorides, particularly NaCl, $CaCl_2$, and $FeCl_2$. This is

**Table 1** Summary of microthermometric data for fluid inclusions in the cavity quartz of the Igarapé Bahia deposit

| Sample | F353/194.20 m | | |
|---|---|---|---|
| Inclusion type[a] | 1 | 2A and 2B | 3A and 3B |
| Number of inclusions | 26 | 32 | 64 |
| Te (°C) | −43 to −65 | −45 to −72 | |
| $Tm_{HH}$ (°C)[b] | −24/−15 | 2 to 22 | |
| $Tm_{ice}$ (°C) | −3 to −46 | −19 to −47 | −8 to −10 |
| $Tm_{CO2}$ (°C) | | | −56.6 to −58.3 |
| $Th_{CO2(L)}$ (°C) | | | −8.2 to 30.9 |
| $Tm_C$ (°C) | | | −7 |
| $Th_{(LV-L)}$ (°C) | 110 to 189 | | |
| $Th_{(SLV-SL)}$ (°C) | | 111 to 220 | |
| $Tm_H$ (°C) | | 168 to 330 | |
| NaCl equiv (wt%)[c] | 5 to 23 | 29 to 41 | 6 to 7 |
| NaCl+$CaCl_2$ equiv (wt%)[d] | 16 to 24 | 32 to 45 | |

*Te* First melting or eutectic melting, $Tm_{HH}$ hidrohalite melting, $Tm_{ice}$ ice melting, $Tm_{CO2}$ $CO_2$ melting, $Th_{CO2(L)}$ $CO_2$ homogenization to liquid, $Tm_C$ clathrate melting, $Th_{(LV-L)}$ homogenization to liquid, $Th_{(SLV-SL)}$ partial homogenization, $Tm_H$ halite melting temperature

[a] *1* Aqueous, diluted, liquid-vapor inclusions; *2A* saline aqueous inclusions, with one or two solids; *2B* saline aqueous inclusions, with more than two solids; *3A* aqueous-carbonic inclusions; *3B* carbonic inclusions

[b] Very few measurements were obtained.

[c] Salinity calculated from $Tm_{ice}$ (Bodnar 1993), from $Tm_H$ (Sterner et al. 1988), and from $Tm_C$ (Chen 1972).

[d] Bulk salinity estimated following the method of Williams-Jones and Samson (1990).

consistent with the nature of the solid phases from type 2 inclusions analyzed by electron microscope, which include dominantly halite cubes, complex Fe–Mn–Na–Ca–Cl phases, together with some Ca and Fe silicates (Fig. 5c).

The vast majority of the $Tm_{ice}$ values obtained for type 1 inclusions are confined within the −22° to −3°C range, with a very few values between −46° and −43°C. Type 2 inclusions have $Tm_{ice}$ values mostly in the −23° to −19°C range, with scattered values from −47° to −29°C (Fig. 6b). Based on the system $H_2O$–NaCl, $Tm_{ice}$ constrains salinities of type 1 inclusions between 5 and 23 wt% NaCl equiv, whereas $Tm_H$ constrains salinities of type 2 inclusions between 29 and 41 wt% NaCl equiv (Fig. 6c). In general, the more $CaCl_2$-enriched inclusion fluids (lowest Te) tend to be the more saline (lower $Tm_{ice}$).

Hydrohalite melting ($Tm_{HH}$) in type 1 inclusions was rarely observed between −24° and −15°C, whereas for type 2 inclusions, only a few values spanning from 2° up to 22°C were recorded, probably indicating the metastable presence of a $CaCl_2$–hydrate. Type 1 inclusions are poorly represented in the $H_2O$–NaCl–$CaCl_2$ ternary diagram due to the lack of reliable $Tm_{HH}$ data, and only those of the high salinity range have been measured (Fig. 6d). In the $H_2O$–NaCl–$CaCl_2$ system, they show bulk salinities that range from 16 to 24 wt% NaCl+$CaCl_2$ equiv, with NaCl and $CaCl_2$ contents that vary from 14 to 24 wt% and from 0 to 7 wt%, respectively, and with NaCl/(NaCl+$CaCl_2$) ratios in the 0.7–1 range.

Total homogenization temperatures ($Th_{(LV-L)}$) recorded for type 1 inclusions from the quartz cavity vary between 110° and 189°C. The type 2 inclusions, most of which of the 2A subtype, display disappearance of the vapor bubble ($Th_{(SLV-SL)}$) between 111° and 220°C and total homogenization, via $Tm_H$, within the 168°–330°C range (Fig. 6e). A halite melting temperature ($Tm_H$) was obtained for only one 2B subtype inclusion in this sample, yielding 301°C, after vapor homogenization at 127°C.

The combination of these microthermometric data with the NaCl–$CaCl_2$–$H_2O$ ternary diagram constrains bulk salinities of type 2 inclusions between 32 and 45 wt% NaCl+$CaCl_2$ equiv, with NaCl and $CaCl_2$ contents that vary from 31 up to 38 wt% and from 0 to 14 wt%, respectively, and with NaCl/(NaCl+$CaCl_2$) ratios of 0.7–1 (Fig. 6d).

The type 3 inclusions contained in the quartz cavity yield a $CO_2$ melting temperature range from −56.6° to −58.3°C, which is lower than the melting temperature of pure $CO_2$ (−56.6°C). This range is consistent with the presence of small concentrations of $CH_4$ in addition to $CO_2$, also detected by Raman spectroscopic analyses. The $CO_2$ homogenization occurs at temperatures that vary widely, from −8.2° to 30.9°C, corresponding to densities of 0.50 to 0.95 g/cm$^3$. A mean salinity of 6 wt% NaCl equiv for the aqueous phase of the 3A inclusions was obtained from clathrate melting temperatures of about 7°C.

## Results from the vein samples

Data obtained from fluid inclusions contained in quartz of five veins that transect the Igarapé Bahia deposit are summarized in Table 2. Inclusions in vein quartz vary between 5 and 20 μm in length and are dominated by the

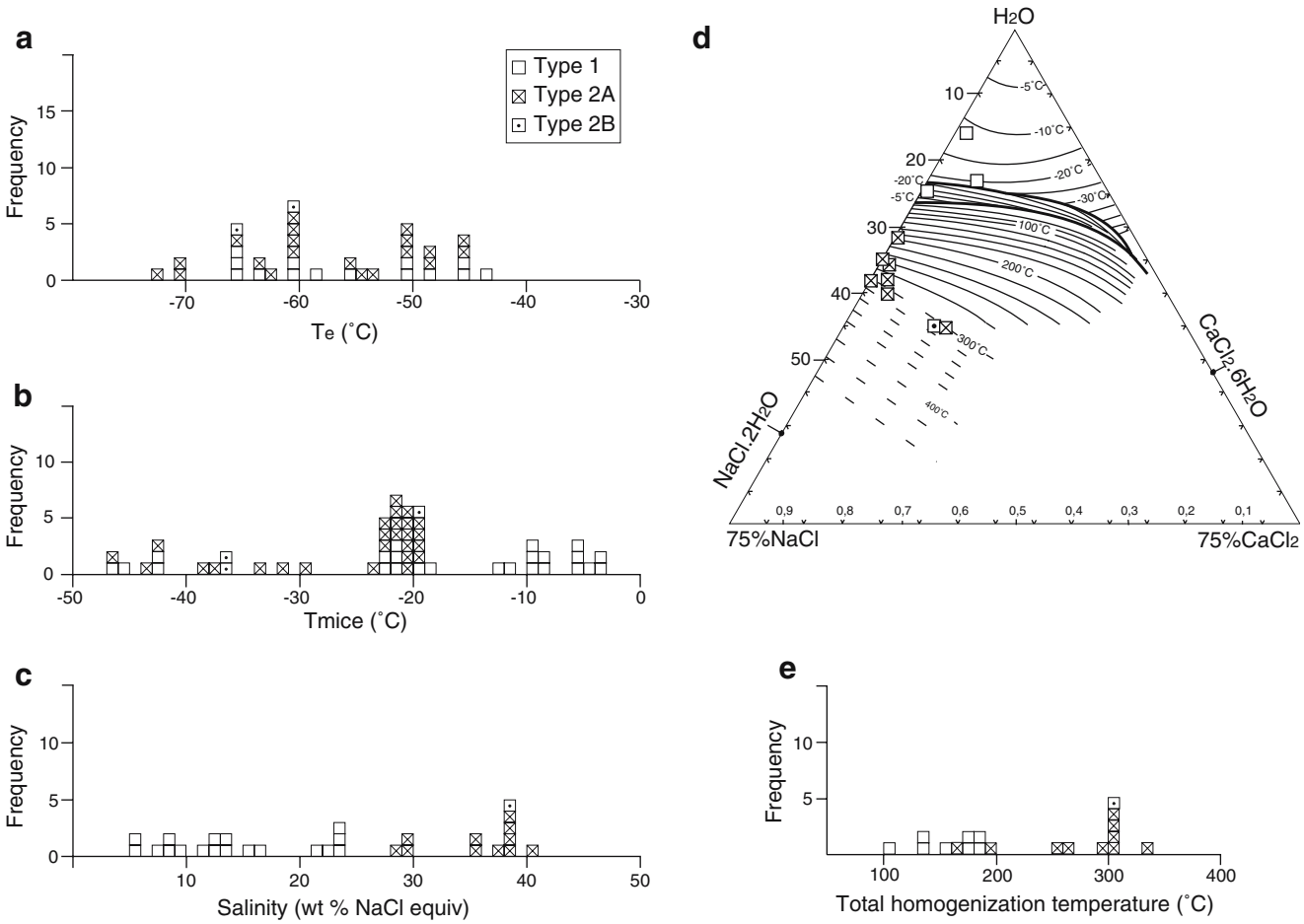


**Fig. 6** Microthermometric data obtained from aqueous fluid inclusions of the cavity quartz (sample F353/194.20 m). Type 1 are aqueous, diluted, liquid–vapor inclusions. Type 2A are saline aqueous inclusions containing one or two solids and a vapor bubble. Type 2B are saline aqueous inclusions containing more than two solids and a vapor bubble. **a** First melting temperatures (Te). **b** $Tm_{ice}$. **c** Salinities (in wt% NaCl equiv) calculated from $Tm_{ice}$ and the equation of Bodnar (1993) for aqueous type 1 inclusions and from halite melting temperatures ($Tm_H$) and the equation of Sterner et al. (1988) for saline aqueous type 2 inclusions. **d** Salinities (in wt% NaCl+$CaCl_2$ equiv) obtained from ice ($Tm_{ice}$), hydrohalite ($Tm_{HH}$), and halite ($Tm_H$) melting temperatures using the method of Williams-Jones and Samson (1990). **e** Total homogenization temperatures obtained from type 1 ($Th_{(LV-L)}$) and type 2 ($Tm_H$) inclusions

aqueous 1, 2A, and 2B inclusion types. The $CO_2$-bearing inclusions are found locally in only one of the veins. Daughter salts in type 2 inclusions are mostly halite (NaCl), but Fe chloride ($FeCl_2$) and some sylvite (KCl) crystals are also present (Fig. 5f). In the vein quartz, these inclusion types occur together in populations that delineate growth zones (Fig. 5e) or form intracrystalline planar arrays, and, accordingly, they are interpreted as of primary and pseudosecondary nature, respectively.

The inclusion types 1 and 2 display Te values mostly between −50° and −70°C, indicating that the aqueous fluids of the veins are also composed mostly of NaCl, $CaCl_2$, and $FeCl_2$ (Fig. 7a). The $Tm_{ice}$ of type 1 inclusions display a wide range of values and a bimodal distribution with strong concentrations between −25° and −15°C (peak at −23°C) and between −10° and −3°C (peak at −8°C; Fig. 7b). $Tm_{ice}$ of type 2 inclusions are strongly concentrated in the range −20° to −27°C (peak at −24°C; Fig. 7b). On the basis of the system $H_2O$–NaCl, salinities for type 1 inclusions range mainly between 8 and 23 wt% NaCl equiv, whereas salinities for type 2A inclusions range mainly from 30 to 40 wt% NaCl equiv (Fig. 7c). Salinities of up to 60 wt% NaCl were calculated for some 2B type inclusions.

In the ternary NaCl–$CaCl_2$–$H_2O$ diagram, the type 1 inclusions display bulk salinities from 10 to 25 wt% NaCl+$CaCl_2$ equiv, with NaCl and $CaCl_2$ contents of 9 to 25 wt% and 0 to 20 wt%, respectively, and with NaCl/(NaCl+$CaCl_2$) ratios between 0.1 and 1 (Fig. 7d).

The homogenization temperatures ($Th_{(LV-L)}$) of the vein type 1 inclusions are confined within the 99°–192°C interval, with a peak at ~150°C, whereas for vein type 2 inclusions, total homogenization takes place by the dissolution of halite ($Tm_H$), after vapor disappearance, at temperature values spanning from 115° up to 519°C, with no resolvable peak (Fig. 7e). The halite melting temperatures ($Tm_H$) combined with the NaCl–$CaCl_2$–$H_2O$ dia-

**Table 2** Summary of the microthermometric data for fluid inclusions in vein quartz of the Igarapé Bahia deposit

| Samples | F382/273.35 m; F382/315.70 m; F332/231.80 m; F332/286.40 m; F375/237.00 m. | | |
|---|---|---|---|
| Inclusion type[a] | 1 | 2A and 2B | 3A and 3B |
| Number of inclusions | 138 | 111 | 11 |
| Te (°C) | −48 to −60 | −35 to −63 | |
| $Tm_{HH}$ (°C) | −17 to −33 | −1 to −27 | |
| $Tm_{ice}$ (°C) | −1 to −27 | −16 to −46 | |
| $Tm_{CO2}$ (°C) | | | −56.6 to −56.7 |
| $Th_{CO2}$ (°C) | | | −4.6 to 29.6 |
| $Th_{(LV-L)}$ (°C) | 99 to 192 | | |
| $Th_{(SLV-SL)}$ (°C) | | 78 to 173 | |
| $Tm_H$ (°C) | | 115 to 519 | |
| NaCl equiv (wt%)[b] | 2 to 23 | 31 to 63 | |
| $NaCl+CaCl_2$ equiv (wt%)[c] | 10 to 25 | 33 to 60 | |

*Te* First melting or eutectic melting, $Tm_{HH}$ hidrohalite melting, $Tm_{ice}$ ice melting, $Tm_{CO2}$ $CO_2$ melting, $Th_{CO2(L)}$ $CO_2$ homogenization to liquid, $Th_{(LV-L)}$ homogenization to liquid, $Th_{(SLV-SL)}$ partial homogenization, $Tm_H$ halite melting temperature

[a] *1* Aqueous, diluted, liquid-vapor inclusions; *2A* saline aqueous inclusions, with one or two solids; *2B* saline aqueous inclusions, with more than two solids; *3A* aqueous-carbonic inclusions; *3B* carbonic inclusions.

[b] Salinity calculated from $Tm_{ice}$ (Bodnar 1993) and from $Tm_H$ (Sterner et al. 1988).

[c] Bulk salinity estimated following the method of Williams-Jones and Samson (1990).

gram yield bulk salinities for type 2 vein inclusions ranging from 33 up to 60 wt% $NaCl+CaCl_2$ equiv (Fig. 7d). In these inclusions, concentrations of NaCl and $CaCl_2$ display values that vary from 19 to 59 wt% and from 1 to 17 wt%, respectively, with $NaCl/(NaCl+CaCl_2)$ ratios between 0.6 and 1 (Fig. 7d).

Type 3 aqueous carbonic inclusions are found locally in one of the veins. The $CO_2$ melting temperatures ($Tm_{CO2}$) concentrate at −56.6°C indicating that the carbonic phase is pure $CO_2$. Homogenization occurs always to the liquid phase ($Th_{CO2(L)}$) at temperatures between −4° and +30°C, indicating variable densities, from 0.6 to 0.95 g/cm$^3$.

## Fluid entrapment processes

Fluids trapped in the quartz cavity are moderate to highly saline aqueous fluids, represented by the inclusion types 1 and 2 and modeled in the system $H_2O$–NaCl–$CaCl_2$–($\pm FeCl_2$), together with $CO_2$–($\pm CH_4$) and low-salinity $H_2O$–$CO_2$–($\pm CH_4$) fluids, represented by the type 3 inclusions. The ubiquitous spatial coexistence of these fluid inclusion assemblages within the same populations strongly suggests that they were simultaneously trapped during the precipitation of the cavity quartz within the timeframe of the Cu–Au mineralizing episode. Although coeval entrapment of the fluid inclusion assemblage has been suggested, this process may have taken place preferentially by in situ mixing of two originally unrelated fluids, giving rise to variable compositions and salinities by the mechanical mixtures of the end-member fluids during heterogeneous trapping. The spatial coexistence and the variable degree of fill shown by the $CO_2$-rich inclusions, on the other hand, suggest that this fluid inclusion assemblage could be the result of unmixing of an originally homogeneous $H_2O$–$CO_2$ fluid. If this is assumed, mixing of the aqueous fluids with the $CO_2$-rich fluids may have probably taken place in the two-phase, subsolvus region of the system $H_2O$–$CO_2$–NaCl. This entrapment model would be similar to that described by Anderson et al. (1992) for mesothermal gold mineralization in the Transvaal Sequence, South Africa. However, total homogenization to the liquid and to the vapor within the same range of temperature could not be assessed due to decrepitation of these inclusions before total homogenization. As a consequence, unmixing cannot be properly confirmed for the $CO_2$-rich fluids in this study.

The unmixing from a single homogeneous $H_2O$–$CO_2$–($\pm CH_4$)–NaCl–$CaCl_2$–($\pm$ $FeCl_2$) fluid over a range of temperature and pressure could also produce similar fluid inclusion assemblages as those described in this study and which would meet part of the basic criteria established by Ramboz et al. (1982) for unmixing. However, in the unmixing process, neither the wide range of composition shown particularly by the aqueous fluids, as suggested by Te values, nor the total homogenization temperature via the dissolution temperature of halite, as shown by the saturated type 2 inclusions, are expected. On the basis of the system $H_2O$–NaCl, the latter microthermometric parameter indicates that the saturated aqueous inclusions homogenize along the halite liquidus and not within the liquid–vapor domain (Bodnar 2003).

Fluids trapped in quartz of five different veins that cut the Igarapé Bahia deposit are predominantly aqueous of moderate to high salinity and belong to the system $H_2O$–NaCl–$CaCl_2$–($\pm$ $FeCl_2$), similar to those of the quartz cavity. However, differently from the quartz cavity, low-salinity $H_2O$–$CO_2$ fluids are rare or absent in the vein quartz.

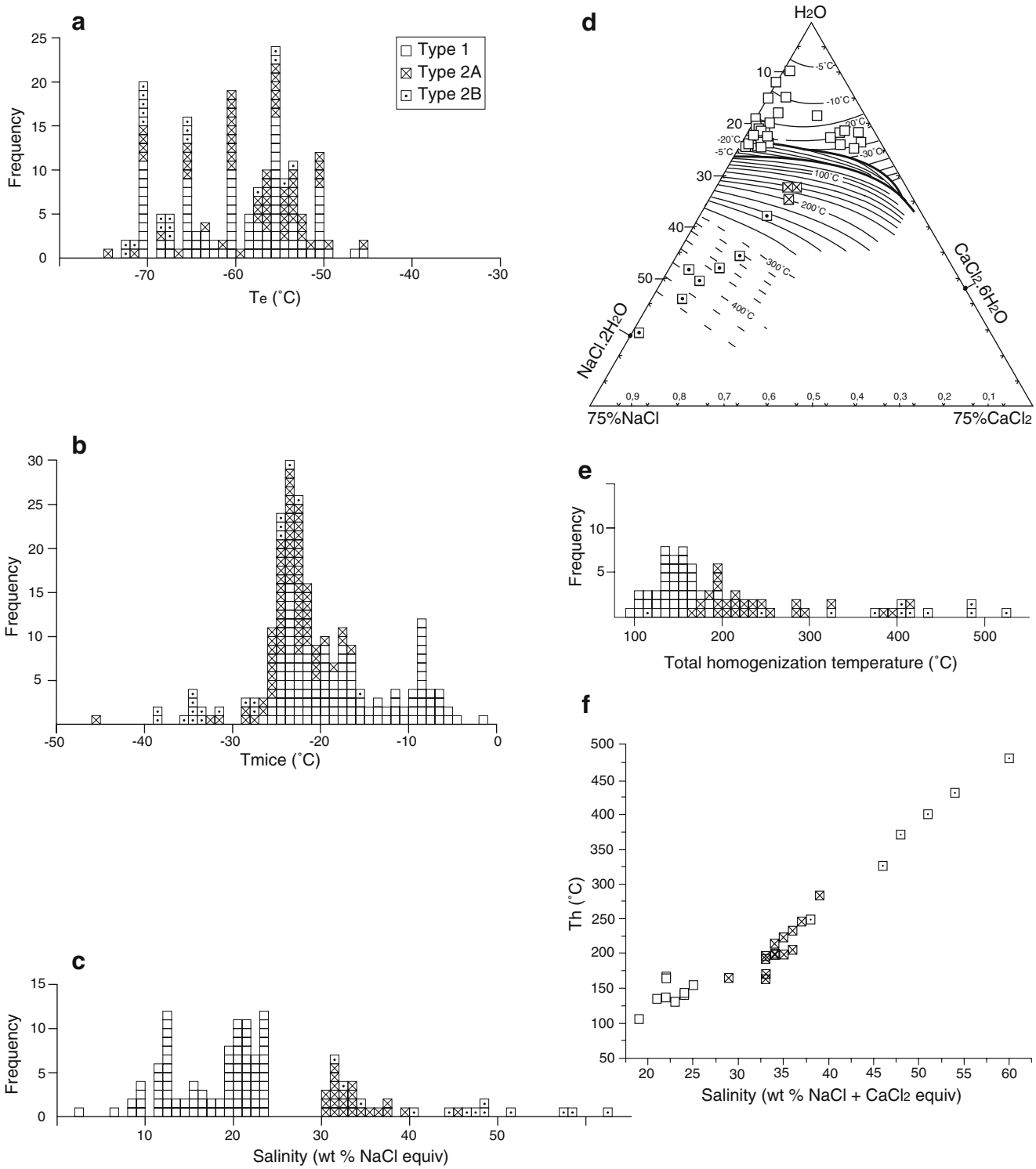


**Fig. 7** Microthermometric data obtained from aqueous fluid inclusions of vein quartz (samples F383/273.35 m, F382/315.70 m, F332/231.80 m, F332/286.40 m, F375/237.00 m). Type 1 are aqueous, diluted, liquid–vapor inclusions. Type 2A are saline aqueous inclusions containing one or two solids and a vapor bubble. Type 2B are saline aqueous inclusions containing more than two solids and a vapor bubble. **a** First melting temperatures (Te). **b** $Tm_{ice}$. **c** Salinities (in wt% NaCl equiv) calculated from $Tm_{ice}$ and the equation of Bodnar (1993) for aqueous type 1 inclusions and from halite melting temperatures ($Tm_H$) and the equation of Sterner et al. (1988) for saline aqueous type 2 inclusions. **d** Salinities (in wt% NaCl+$CaCl_2$ equiv) obtained from ice ($Tm_{ice}$), hydrohalite ($Tm_{HH}$), and halite ($Tm_H$) melting temperatures using the method of Williams-Jones and Samson (1990). **e** Total homogenization temperatures obtained from type 1 ($Th_{(LV-L)}$) and type 2 ($Tm_H$) inclusions. **f** Homogenization temperatures (Th) against salinity (in wt% NaCl+$CaCl_2$ equiv)

Homogenization temperatures plotted against bulk salinity values for these aqueous fluids display a clear correlation trend of decreasing temperature and salinity, which may have been attained by fluid mixing, similarly to the entrapment process described for the quartz cavity (Fig. 7f).

Within this fluid-mixing scenario, the involvement of fluids of different compositions, including high-salinity and $H_2O$–$CO_2$ systems, and of variable total homogenization temperatures, precludes the estimate of the trapping temperature for both the quartz cavity and vein fluids. In this context, even with an independent geothermometer, as provided by the stable isotope data in this study (see below), no pressure correction can be obtained with an adequate degree of certainty, as these fluids yield a wide range of isochores, with varying slopes in P–T space. Additionally, isochores for high salinity inclusions containing various amounts of salt chlorides and that show total homogenization via the dissolution of a salt, as in the case of the type 2 inclusions, have not been determined, as their volumetric properties are poorly constrained (Bodnar 2003).

## Stable isotope study

Samples for the stable isotope study were selected from the mineralized fragmental unit and also from the veins that transect the Igarapé Bahia deposit. The C and O isotope analyses of carbonates were performed on samples of siderite-rich fragmental rocks and on vein carbonate separates. The S isotope analyses were undertaken on chalcopyrite grains selected from the ore layer, from the hanging wall metarhythmites, and from veins. Additional O isotope study was carried out on quartz and magnetite separates both from the ore unit and from the veins.

### Carbon and oxygen isotopes in carbonates

The $\delta^{13}C$ and $\delta^{18}O$ results obtained on 25 samples of the fragmental rock and vein carbonates, together with the carbonate varieties identified in each sample, are shown in Tables 3 and 4. The $\delta^{13}C$ and $\delta^{18}O$ results are given in Peedee belemnite (PDB) and standard mean ocean water (SMOW) notation, respectively. The siderites, which are the dominant carbonate species in the fragmental rock matrix, display $\delta^{13}C$ values from −13.4 to −8.3 per mil and $\delta^{18}O$ values ranging from 9.3 to 20.7 per mil. Less common phases, like ankerite and calcite, have consistently more positive $\delta^{13}C$ values, from −8.7 to −6.7 per mil, and more negative $\delta^{18}O$ values, from 4.7 to 8.9 per mil (Fig. 8a). The vein carbonates present $\delta^{13}C$ data for calcite and other minor phases, like ankerite, dolomite, and siderite, distributed in the range −15.6 to −6.7 per mil, with corresponding $\delta^{18}O$ values of 1.2 to 14.1 per mil (Fig. 8b).

The $\delta^{13}C$ and $\delta^{18}O$ results of this study partly overlap with data previously obtained on carbonates of Igarapé Bahia by Tazava (1999) and Villas et al. (2001), except for the more $\delta^{13}C$-depleted and $\delta^{18}O$-enriched values determined for siderites in this study.

According to their $\delta^{13}C$ composition, carbonates from both fragmental rocks and veins can be tentatively separated into two groups. The first group is constrained by $\delta^{13}C$ values between −6 and −8 per mil, which includes most of the vein carbonates and ankerite and calcite from the fragmental layer. This range suggests a deep-seated or magmatic source for the $CO_2$ carbon, which is characterized by $\delta^{13}C$ values from −3 to −8 per mil, with a mean at −6 per mil, according to Taylor (1986: field 4, Fig. 8a). However, as pointed out by Kerrich (1990), hydrothermal carbonates of this same compositional range may also result from leaching of sedimentary carbonates or oxidation of free carbon, and do not necessarily indicate that the $CO_2$ is of mantle or magmatic origin. The other group includes $\delta^{13}C$ results from −8 to −15 per mil, which is dominated by the siderites of the fragmental rocks and, subordinately, by some ankerite and calcite of the veins. These numbers indicate that the carbonates incorporated $CO_2$ produced by the oxidation or hydrolysis of organic matter, typically low in $\delta^{13}C$ (field 5, Fig. 8a). Traces of fossil microorganisms and graphite have been identified in Archean BIF layers of the Carajás Province (e.g., Macambira 1992; Winter 1994; Lindenmayer et al. 2001), and small concentrations of $CH_4$ were detected in fluid inclusions by Raman spectroscopy in the present study. This reinforces the role of organic matter as one of the sources of carbon to the mineralizing fluids of Igarapé Bahia.

The large variation ranges of the $\delta^{18}O$ data, from 20.7 to 4.7 per mil in carbonates of the fragmental rocks and from 14.1 to 1.2 per mil in the vein carbonates (Fig. 8a,b), define important $\delta^{18}O$ depletion trends, which may be related to fluid mixing as indicated from the fluid inclusion study. Fluid regimes, in both cases, would be initially dominated by $\delta^{18}O$-enriched fluids, either magmatic or fluids that interacted with $^{18}O$-rich rocks at high temperatures. The shift towards lower $\delta^{18}O$ values may have been attained by increasing infiltration of cooler solutions into the systems. In the case of the veins, mixing with $\delta^{18}O$-depleted, meteoric fluids seems evident.

### Sulfur isotopes

The $\delta^{34}S$ isotopic values obtained from 26 samples of chalcopyrite from the fragmental rock matrix, from nodules and layers in metarhythmites, and from veins are presented in Tables 3 and 4, with results given in Canyon Diablo troilite (CDT) notation.

The $\delta^{34}S$ values obtained for chalcopyrite from the three orebodies of Igarapé Bahia and from the metarhythmites are

**Table 3** Stable isotope data of whole-rock samples and mineral separates from the mineralized fragmental rock unit of the Igarapé Bahia deposit, including calculated temperatures and fluid compositions

| Sample number | Rock type | Mineral | $\delta^{18}O$‰ SMOW | $\delta^{13}C$‰ PDB | $\delta^{34}S$‰ CDT | Temperature (°C) | $\delta^{18}O_{H2O}$ SMOW |
|---|---|---|---|---|---|---|---|
| F332/237.20 m(a) | Fragm. rock | Sd | 17.5 | −11.2 | | | 13.3[a] |
| F332/237.20 m(b) | Fragm. rock | Sd | 14.4 | −10.3 | | | 10.2[a] |
| F332/247.70 m(b) | Fragm. rock | Sd | 20.7 | −12.0 | | | 16.5[a] |
| F332/256.80 m | Fragm. rock | Sd | 14.6 | −12.1 | | | 10.4[a] |
| F332/260.97 m | Fragm. rock | Sd | 12.5 | −10.9 | | | 8.3[a] |
| F332/275.57 m | Fragm. rock | Sd | 16.5 | −13.4 | | | 12.3[a] |
| F345/191.20 m | Fragm. rock | Sd | 20.3 | −13.2 | | | 16.1[a] |
| F382/225.50 m | Fragm. rock | Ank | 8.7 | −7.4 | | | |
| | | Cal | 8.1 | −7.7 | | | |
| F382/239.50 m | Fragm. rock | Ank | 8.3 | −6.7 | | | |
| F382/286.60 m | Fragm. rock | Sd | 9.2 | −8.3 | | | 5.0[a] |
| | | Ank | 8.9 | −7.8 | | | |
| F382/316.25 m(b) | Fragm. rock | Ank | 5.8 | −7.5 | | | |
| | | Cal | 4.9 | −7.9 | | | |
| F382/353.15 m | Fragm. rock | Ank | 6.7 | −8.2 | | | |
| | | Cal | 7.8 | −8.1 | | | |
| F382/362.30 m | Fragm. rock | Ank | 4.6 | −8.6 | | | |
| | | Cal | 5.9 | −8.6 | | | |
| F332/259.10 m | Fragm. rock | Ccp | | | 4.6 | | |
| F345/189.50 m | Fragm. rock | Ccp | | | 3.0 | | |
| F345/205.80 m | Fragm. rock | Ccp | | | 0.5 | | |
| F346/220.15 m | Fragm. rock | Ccp | | | 1.7 | | |
| F346/245.20 m | Fragm.rock | Ccp | | | 4.7 | | |
| F353/177.35 m | Fragm. rock | Ccp | | | 1.8 | | |
| F353/184.12 m | Fragm. rock | Ccp | | | 5.5 | | |
| F353/227.60 m | Fragm. rock | Ccp | | | −10.8 | | |
| F382/206.60 m | Fragm. rock | Ccp | | | 2.8 | | |
| F382/360.70 m | Fragm. rock | Ccp | | | 5.6 | | |
| F392/334.00 m | Fragm. rock | Ccp | | | 4.1 | | |
| F14D/150.00 m | Layer in turb. | Ccp | | | −1.1 | | |
| F353/158.40 m | Nodule in turb. | Ccp | | | −0.9 | | |
| F392/159.85 m | Nodule in turb. | Ccp | | | 0.4 | | |
| F392/177.80 m | Nodule in turb | Ccp | | | 0.2 | | |
| F392/318.50 m | Nodule in turb. | Ccp | | | 0.0 | | |
| F332/259.10 m | Fragm. rock | Mag | −1.4 | | | 313[b] | 6.5[c] |
| F353/184.12 m | Fragm. rock | Mag | 2.3 | | | 416[b] | 9.1[c] |
| F353/227.60 m | Fragm. rock | Mag | 3.3 | | | 453[b] | 9.7[c] |
| F382/206.80 m | Fragm. rock | Mag | 1.9 | | | 403[b] | 8.8[c] |
| F382/360.40 m | Fragm. rock | Mag | −1.1 | | | 323[b] | 6.5[c] |
| F382/360.70 m | Fragm. rock | Mag | 0.0 | | | 349[b] | 7.5[c] |
| F392/334.00 m | Fragm. rock | Mag | 4.0 | | | 483[b] | 10.2[c] |
| F353/194.20 m | Quartz cavity | Quartz | 12.8 | | | 416[b] | 9.1[c] |

*Fragm. rock* Fragmental rock, *turb* turbidite, *sd* siderite, *ank* ankerite, *cal* calcite, *ccp* chalcopyrite, *mag* magnetite

[a] Calculated from the equation siderite–$H_2O$ of Zheng (1999) using a temperature of 400°C.

[b] Calculated using fractionation equations of Matsuhisa et al. (1979) and Bottinga and Javoy (1973) and by assuming that quartz of sample F353/194.20 m is in equilibrium with all the magnetite samples.

[c] Calculated from the equations magnetite–$H_2O$ of Bottinga and Javoy (1973) and quartz–$H_2O$ of Matsuhisa et al. (1979).

concentrated in the range −1.1 to 5.6 per mil, with an outlier at −10.8 per mil (Fig. 9a). The vein chalcopyrites show a narrower range, from −0.3 to 4.0 per mil (Fig. 9b).

The $\delta^{34}S$ results for chalcopyrites from the ore layer and metarhythmites of Igarapé Bahia partly overlap with $\delta^{34}S$ data between −2.1 and 4.6 per mil obtained earlier by Villas et al. (2001) on sulfides of the same deposit.

The clustering of $\delta^{34}S$ values between 0 and 2 per mil shown in Fig. 9a indicates that most sulfur is magmatic, either derived directly from a magmatic source or from

**Table 4** Stable isotope data of mineral separates from veins of the Igarapé Bahia deposit, including calculated temperatures and fluid compositions

| Sample number | Rock type | Mineral | $\delta^{18}O$‰ SMOW | $\delta^{13}C$‰ PDB | $\delta^{34}S$ ‰ CDT | Temperature (°C) | $\delta^{18}O_{H2O}$ SMOW[(2)] |
|---|---|---|---|---|---|---|---|
| F14D/219 m | Vein in mafic rock | Ank | 8.2 | −15.6 | | | |
| | | Cal | 9.7 | −12.4 | | | |
| F14D/287 m | Vein in turb. | Ank | 7,9 | −10.1 | | | |
| | | Cal | 7.9 | −9.7 | | | |
| F14D/503 m | Vein in turb. | Dol | 8.7 | −7.8 | | 207[a] | |
| | | Cal | 9.3 | −7.9 | | | |
| F332/247.70 m(a) | Vein in fragm. rock | Sd | 11.9 | −9.5 | | | |
| F332/307.35 m | Vein in mafic dike | Cal | 5.7 | −8.8 | | | |
| F327/388.60 m | Vein in meta-arenite | Cal | 2.3 | −8.0 | | | |
| F353/188.07 m | Vein in turb. | Cal | 14.0 | −7.2 | | | |
| F356/396.20 m | Vein in metabasalt | Cal | 1.1 | −8.0 | | | |
| F375/1218.20 m | Vein in mafic dike | Cal | 5.2 | −7.9 | | 259[a] | |
| F382/273.35 m | Vein in fragm. rock | Ank | 8.6 | −7.2 | | | |
| | | Sd | 10.7 | −6.6 | | | |
| F382/315.70 m | Vein in fragm. rock | Ank | 7.8 | −7.9 | | 207[a] | |
| | | Sd | 8.9 | −7.9 | | | |
| | | Cal | 7.5 | −7.8 | | | |
| F382/316.25 m(a) | Vein in fragm. rock | Ank | 6.8 | −8.0 | | | |
| | | Cal | 81 | −7.9 | | | |
| F14D/480 m | Vein in metabasalt | Ccp | | | 1.4 | | |
| F327/388.60 m | Vein in meta-arenite | Ccp | | | 0.8 | | |
| F332/286.45 m | Vein in meta-arenite | Ccp | | | −0.3 | | |
| F353/193.15 m | Vein in fragm. rock | Ccp | | | 3.0 | | |
| F375/237.40 m | Vein in mafic dike | Ccp | | | 0.1 | | |
| F375/1207.30 | Vein in mafic dike | Ccp | | | −0.3 | | |
| F382/249.70 m | Vein in fragm.rock | Ccp | | | 0.7 | | |
| F382/273.35 m | Vein in fragm. rock | Ccp | | | 4.0 | | |
| F382/281.10 m | Vein in fragm. rock | Ccp | | | 3.2 | | |
| F382/315.70 m | Vein in fragm. rock | Ccp | | | 4.0 | | |
| F14D/503 m | Vein in turb. | Quartz | 11.3 | | | 207[a] | 0.2[b] |
| F332/231.80 m | Vein in meta-arenite | Quartz | 2.6 | | | | |
| F332/286.45 m | Vein in meta-arenite | Quartz | 9.4 | | | | |
| F345/284.00 m | Vein in metabasalt | Quartz | 9.9 | | | | |
| F346/242.15 m | Vein in fragm. rock | Quartz | 11.8 | | | | |
| F382/273.35 m | Vein in fragm. rock | Quartz | 10.0 | | | | |
| F382/315.70 m | Vein in fragm. rock | Quartz | 9.5 | | | 207[a] | −1.6[b] |
| F392/211.45 m | Vein in turb. | Quartz | 11.1 | | | | |
| F375/1218.20 m | Vein in mafic dike | Mag | −10.6 | | | 259[a] | 1.8[b] |

[a] Calculated using fractionation equations of Bottinga and Javoy (1973), Friedman and O'Neil (1977), and Matsuhisa et al. (1979).
[b] Calculated from the equations magnetite–$H_2O$ of Bottinga and Javoy (1973) and quartz–$H_2O$ of Matsuhisa et al. (1979).
*turb* Turbidite, *fragm.* rock fragmental rock, *ank* ankerite, *cal* calcite, *dol* dolomite, *sd* siderite, *ccp* chalcopyrite, *mag* magnetite

nonmagmatic fluids that leached sulfides from magmatic rocks. Additionally, the histogram in Fig. 9a indicates that other sulfur sources contributed to the Igarapé Bahia chalcopyrites. The extreme value of −10.8 per mil indicates a limited, although important, contribution of reduced, biogenic sulfur. This reinforces the negative $\delta^{13}C$ values down to −13 per mil obtained for the siderites, which also indicate entrainment of organic matter in the fluid phase. The higher $\delta^{34}S$ values of 3 to 5.6 per mil, on the other hand, indicate the participation of oxidized sulfur, which could be produced by inorganic, high-temperature reduction of sea-water sulfate or of sulfate from a sedimentary source.

The vein chalcopyrites show a distribution of $\delta^{34}S$ values (−0.3 to 4.0 per mil; Fig. 9b) that is narrower than

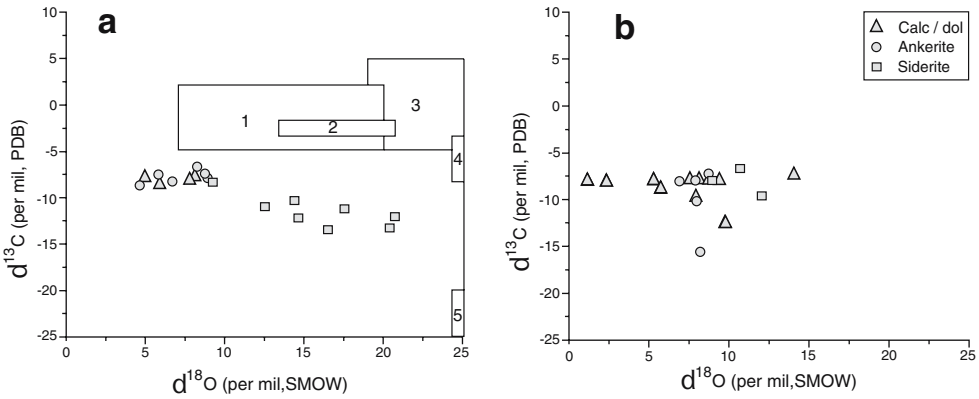


**Fig. 8** Del$^{13}$C versus $\delta^{18}$O diagram for the Igarapé Bahia carbonates. **a** Results of carbonates from the fragmental ore layer. Also included in this diagram are the following fields: 1=carbonates of VHMS deposits (Huston 1999); 2=Olympic Dam siderites (Oreskes and Einaudi 1992); 3=marine carbonates (Rollinson 1995); 4=deep-seated carbon (Taylor 1986); 5=organic carbon (Rollinson 1995). **b** Results of carbonates from the veins

the variation presented by the sulfides of the fragmental layer and metarhythmites. This range suggests that sulfur is dominantly magmatic or leached from magmatic rocks.

## Oxygen isotopes and fluid compositions

Apart from the carbonates, magnetite and quartz were also analyzed for $\delta^{18}$O. Magnetite is abundant in the fragmental rock matrix, whereas quartz is usually too fine-grained to be separated, so that only the one sample of coarse quartz from the cavity was analyzed. From the veins, on the contrary, several quartz samples and only one magnetite sample were analyzed. The $\delta^{18}$O data are shown in Tables 3 and 4, with results given in SMOW notation.

The magnetites from the fragmental rock display $\delta^{18}$O values between −1.4 and 4.0 per mil, with a mean at 1.3 per mil. The only quartz sample analyzed from the fragmental rocks returned a $\delta^{18}$O result of 12.8 per mil. The temperatures and fluid compositions obtained from quartz and magnetite $\delta^{18}$O values were calculated by assuming that the only quartz analyzed was in equilibrium with the different analyzed magnetites (Table 3). Using the fractionation equations of Matsuhisa et al. (1979) and Bottinga and Javoy (1973) for quartz–magnetite pairs, temperatures of 313° to 483°C were estimated, with an average of 394°C. This average is consistent with the temperature of ~400°C estimated for the paragenesis of Fe–actinolite–hastingsite–stilpnomelane–magnetite present in the ore unit. The isotopic composition of the mineralizing fluids, calculated from the temperature estimates and the equations of Bottinga and Javoy (1973) and Matsuhisa et al. (1979) resulted in a range of $\delta^{18}O_{fluid}$ from 6.5 to 10.2 per mil. Textural observations made in the ore-bearing fragmental rocks indicate that siderite developed later than magnetite and silicates and consequently was not in equilibrium with these minerals. However, if the $\delta^{18}$O values of the siderites (from 9.2 to 20.7 per mil, Table 3) are considered in equilibrium with a fluid at a similar temperature of 400°C, a larger range of $\delta^{18}O_{fluid}$, from 5.0 to 16.5 per mil, is obtained for the ore fluids by using the fractionation equation of Zheng (1999).

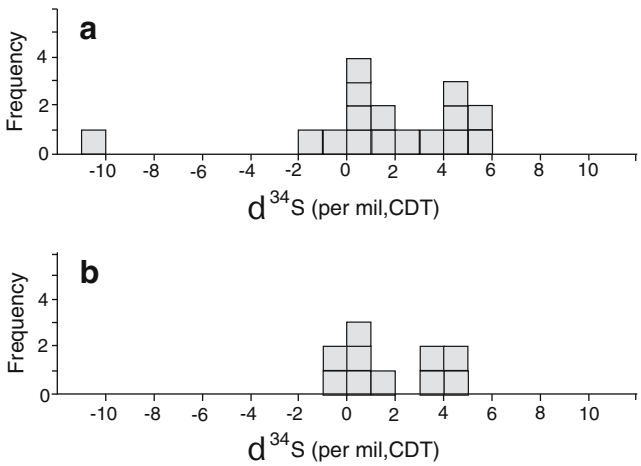


**Fig. 9** Histograms of $\delta^{34}$S results of chalcopyrite of Igarapé Bahia. **a** Chalcopyrite from the fragmental rock unit and from nodules and thin layers in the hanging wall metarhythmites. **b** Chalcopyrite from veins

The $\delta^{18}$O compositions from 5.0 to 16.5 per mil estimated for the fluid that circulated through the fragmental unit of Igarapé Bahia are very $\delta^{18}$O-enriched, and two possible sources can be considered. The lower part of the range partly coincides with that of magmatic fluids ($\delta^{18}$O of 5.5 to 10 per mil, according to Taylor 1986, Fig. 10) and may indicate the presence of magmatic components in the hydrothermal fluid. The upper part of the range, in turn, suggests a possible interaction with sedimentary rocks, which typically have high $\delta^{18}$O values (Hoefs 1987).

Quartz from the veins presents $\delta^{18}$O values between 9.4 and 11.8 per mil, except for one sample that has a $\delta^{18}$O of 2.6 per mil (Table 4). The only magnetite sample from the veins produced a $\delta^{18}$O result of −10.6 per mil. Equilibrium temperatures for quartz–calcite and magnetite–calcite pairs of three of these veins were calculated from the equations of Matsuhisa et al. (1979), Friedman and O'Neil (1977), and Bottinga and Javoy (1973). The estimated temperatures range from 207° to 259°C and correspond roughly to an average of the homogenization temperatures measured

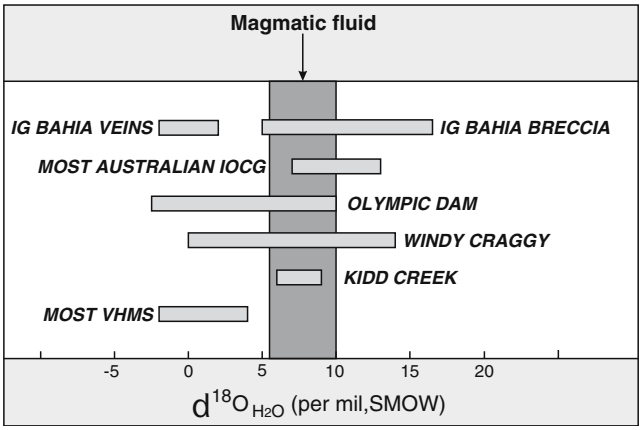


**Fig. 10** Del$^{18}$O diagram showing the range of fluid compositions of the Igarapé Bahia fragmental rock and veins and the ranges of fluids from other deposits and reservoirs. Fluids of most VHMS deposits (Huston 1999); range of Kidd Creek fluids (Beaty et al. 1988); range of Windy Craggy deposit fluids (Peter and Scott 1999); range of Olympic Dam fluids (Oreskes and Einaudi 1992); range of most other Australian Proterozoic IOCG deposits (Williams et al. 2005); range of magmatic fluids (Taylor 1986)

during microthermometric analyses of the veins. The fluid compositions, estimated by using the equations of Bottinga and Javoy (1973) and Matsuhisa et al. (1979), vary between $\delta^{18}O_{fluid}$ of −1.6 and 1.8 per mil.

The calculated temperatures (200°–300°C) and the isotopic composition of the mineralizing fluids ($\delta^{18}O$ around 0 per mil, Fig. 10) of the veins show a pattern that is distinct from that of the fragmental ore layer of Igarapé Bahia, with low $\delta^{18}O_{fluid}$ values that suggest an important contribution from meteoric fluids to the veins.

## Discussion

Genetic models proposed for Igarapé Bahia have involved contrasting syngenetic and epigenetic interpretations. The syngenetic interpretation (Ferreira Filho 1985; Zang and Fyfe 1995; Almada and Villas 1999; Villas and Santos 2001; Dreher 2004) considers Igarapé Bahia as a volcanic-hosted massive sulfide (VHMS) or volcanogenic sulfide deposit, based mainly on geological aspects such as the volcano-sedimentary context of the deposit, stratabound character, and strong chloritic alteration associated with the footwall basaltic host rocks. The epigenetic view (Huhn and Nascimento 1997; Tazava and Oliveira 2000; Ronzé et al. 2000; Santos 2002; Laux et al. 2003; Tallarico et al. 2005) suggests that Igarapé Bahia belongs to the IOCG class of deposits as defined by Hitzman et al. (1992) based mainly on geochronological data and on geochemical features, such as the metallic (Fe oxide, Cu, Au, U, LREE) association of the ore, and the highly saline composition of the ore-related hydrothermal fluids.

As indicated above, the main attributes used in each of the models, that is, geological features on one side and geochronologic and geochemical features on the other, are diverse and will, therefore, be discussed separately.

### Geological features

The geologic environment in which the Itacaiúnas Supergroup host rocks were deposited is considered of prime importance in the syngenetic interpretation (Villas and Santos 2001; Dreher 2004). The volcano-sedimentary setting of these rocks is appropriate for the generation of exhalative deposits, as demonstrated by the extensive banded-iron formations that occur in the Carajás region. These rocks formed in a submarine setting with associated volcanism. The footwall host rocks of the Igarapé Bahia deposit are mafic flows, with accompanying hyaloclastite, autobreccia, BIF and chert layers that indicate a marine environment. The hanging-wall rocks were equally formed in a subaqueous setting, as indicated by the presence of turbidites and, again, associated BIF and chert beds. The location of the ore unit at the interface between the volcanic and sedimentary sequences is also characteristic of syngenetic deposits, which generally develop in horizons that represent changes, either in composition of the volcanic rocks, or changes from volcanism to sedimentation, or even pauses in volcanism (Evans 1995). The ore-bearing fragmental rock unit of Igarapé Bahia is considered in the syngenetic model as a submarine debris flow deposit (Almada and Villas 1999; Villas and Santos 2001) that accumulated besides an ancient growth fault (Dreher and Xavier 2001; Dreher et al. 2005). Evidence for the existence of such faults at the deposit site is given by the debris flow unit and the turbidites themselves, both considered as mass flow deposits (Einsele 1991), and by the abundant slump, disruption, and brecciation features shown by these rocks, indicative of tectonic instability. Geologically similar breccias are described from the Itacaiúnas Supergroup-hosted Pojuca Cu–Zn deposit by Winter (1994). According to Dreher and Xavier (2001), mineralization at Igarapé Bahia probably occurred by subseafloor stratabound infilling and replacement of the debris flow matrix, shortly after deposition, when the sediment was still porous and permeable.

From the epigenetic standpoint, the fragmental rocks are hydraulic or hydrothermal breccias, which were emplaced vertically and explosively at the contact between different lithologies (Tallarico et al. 2005), lacking, therefore, any genetic or temporal relation with the formation of their wallrocks. Mineralization would have occurred concomitantly with brecciation, long after the formation of the host rocks. Hydraulic breccias are commonplace in IOCG

deposits, Olympic Dam being one of the most outstanding examples of mineralization associated with this type of breccia. One aspect considered relevant in this respect is the upright position of the Igarapé Bahia deposit and its semicircular form in plan view, similar to a ring complex and suggestive of the presence of a granitic or alkaline intrusive body at depth (Tallarico et al. 2005).

According to the syngenetic interpretation, the upright position of the fragmental unit, with dips of around 80°, is a concordant structural feature, as these steep dips, besides being identical to those of the wallrocks themselves, are also quite common in other volcano-sedimentary sequences of the Itacaiúnas Supergroup. In the Salobo Cu–Au deposit, for instance, dips of 85° have been described (Réquia and Fontboté 2000), whereas at the Pojuca Cu–Zu deposit dips vary from 50° to 90° (Winter 1994). The nearly vertical position at Igarapé Bahia may have originated essentially through tilting, and the semicircular shape in plan may conceivably reflect the original morphology of the sedimentary layer, combined with displacements caused by faults in both extremities of the orebody.

Other similarly important features for a syngenetic model are the foliated structures of most of the fragmental rocks at Igarapé Bahia and the concordant or parallel foliation in rock fragments and matrices (Fig. 4e–g). This indicates that the fragmental rocks were formed before deformation. The nonfoliated, fine granoblastic texture of the BIF (Fig. 4h) and chert fragments contained in the breccia is typical of metamorphosed chert or quartz–magnetite rocks (Klein 1973), which commonly recrystallize but do not develop other silicate minerals that could impart a fabric to these rocks upon metamorphism.

## Geochronology

Several age determinations were performed on the Igarapé Bahia ore to determine the age of mineralization. Most of the geochronological data is based on Pb-Pb isotope analyses of sulfide and gold grains, with mostly imprecise age results, attributed to radiogenic lead contamination from the host rocks. The Pb-Pb ages on chalcopyrite, from 2,754±36 to 2,777±22 Ma, obtained by Galarza (2002) have significant error margins and cannot be used to precisely constrain the age of mineralization. The Pb-Pb datings performed by Santos (2002) on gold and chalcopyrite particles from the Alemão orebody, with ages between 2,521±56 and 2,595±200 Ma, also display large analytical errors. New Pb-Pb age determinations at 2,744±12 Ma on gold particles of Igarapé Bahia (Galarza et al. 2006) are also considered as not sufficiently precise to support a syngenetic viewpoint, although a link to the mafic volcanic processes that occurred around 2,750 Ma in the Carajás region is suggested. The SHRIMP II U-Pb dating at 2,575±12 Ma performed by Tallarico et al. (2005) on hydrothermal monazite from the matrix of the ore-bearing breccia represents, by far, the best documented and precise age determination. According to Tallarico et al. (2005), this age confirms that mineralization at Igarapé Bahia is epigenetic and temporally related to the Archean (ca. 2,570 Ma) Estrela-type granites of Carajás.

Although robust and significant, the 2,575 Ma age determination by Tallarico et al. (2005) has to be compared with geological data presented in this study and with geological and geochronological information from the existing literature on the Carajás region. In the first place, there are no known granite intrusions in the Igarapé Bahia deposit area, the nearest one being the 1,879±6 Ma Breves intrusion (Tallarico et al. 2004) situated 9 km north. Secondly, the correlation of the Igarapé Bahia mineralization to the Estrela-type granites made by Tallarico et al. (2005) is based on a Rb–Sr age of 2,527±34 Ma obtained for the Estrela granite by Barros et al. (1992). This granite was later redated, using the Pb-Pb method on zircon, at 2,763±7 Ma (Barros et al. 2001, 2004). The only example of 2,570 Ma granites in Carajás is the Old Salobo granite, dated at 2,573±2 Ma (U–Pb zircon, Machado et al. 1991), which is a very small pluton that occurs in the vicinity of the Salobo Cu–Au deposit. Additionally, geological data collected at Igarapé Bahia indicate that the ore-bearing fragmental rocks are mostly foliated rocks that were consequently formed before deformation. If formed at 2,575 Ma, the fragmental rocks would probably lack a tectonic fabric because this age represents a period of tectonic extension at Igarapé Bahia, marked by the intrusion of several mafic dikes (maximum age of ~2,670 Ma, Tallarico et al. 2005), which do not show any sign of penetrative deformation. Furthermore, the geological section presented in Fig. 3a shows that the mineralized fragmental rocks do not transect the Águas Claras Formation meta-arenites that cover the Alemão orebody, whereas the mafic dikes do. This demonstrates that the fragmental rocks must be older than 2,575 Ma. It should also be noted that no mineralized fragmental rock similar to the Igarapé Bahia rocks has so far been observed in the Águas Claras unit. This reinforces the idea that the fragmental rocks were formed before the deposition of the Águas Claras sediments, being therefore coeval with, or close in age to, the Igarapé Bahia Group volcano-sedimentary rocks.

Thus, considering the various geological constraints mentioned above, the monazite age of 2,575±12 Ma obtained by Tallarico et al. (2005) could probably represent a later hydrothermal episode at Igarapé Bahia and not necessarily the main mineralization event. According to Schandl and Gorton (1991), monazite is a reliable geochronometer for U–Pb dating of epigenetic hydrothermal ore deposits because it has a blocking temperature of ~700°C

that prevents resetting, except under high metamorphic conditions. However, newly-formed monazites may develop in ore deposits, either from superimposed hydrothermal events or from fluids derived from metamorphism (Davis et al. 1994). On the other hand, Ayers et al. (2004) demonstrate that monazite is actually susceptible to alteration by acidic or alkaline fluids, which can recrystallize preexisting monazites or precipitate monazite. Therefore, a possibility to consider is that the 2,575 Ma monazite age (Tallarico et al. 2005) is related to fluid circulation associated with a regional transpressional event that occurred around 2,600 Ma in the Carajás region (Holdsworth and Pinheiro 2000).

## Geochemical features

### *Mineralizing fluids*

One of the most important features that Igarapé Bahia shares with IOCG deposits relates to the highly saline mineralizing fluids of up to 45 wt% NaCl+$CaCl_2$ equiv, as determined in this study. This feature is uncommon in syngenetic VHMS-type deposits, which are normally formed from low salinity solutions (Franklin 1993; Sangster 1999). Additionally, the fluid inclusion study revealed that the ore unit was in fact percolated by an assemblage of aqueous fluids of variable salinities and salt compositions. The mentioned aqueous fluids apparently coexisted with carbonic ($CO_2 \pm CH_4$) fluids and low-salinity (6 wt% NaCl equiv) aqueous carbonic fluids. Similarly complex assemblages are described from IOCG deposits such as Olympic Dam and Ernest Henry (Williams et al. 2005). According to Pollard (2006), hydrothermal fluids made up of combinations of $H_2O$–$CO_2$–salts would have a genetic connection to oxidized, potassic granitoids.

### *Metallic association*

Another important feature shared with IOCG deposits concerns the ore mineralogy, which at Igarapé Bahia is dominated by chalcopyrite and magnetite, with scarce pyrite. Syngenetic deposits contain mainly Fe sulfides, like pyrite and pyrrhotite, associated with Cu, Zn, (±Pb) sulfides (Franklin 1993). The elevated concentrations of elements such as P, F, U, and LREE present at Igarapé Bahia (Tallarico et al. 2005) are also absent from volcanogenic deposits but constitute a distinctive geochemical feature of many IOCG deposits (Williams et al. 2005). The mentioned association of elements has led some authors (e.g., Groves and Vielreicher 2001; Tallarico et al. 2005) to suggest a link between the Igarapé Bahia mineralization and alkaline rocks or mantle-sourced fluids.

### *Stable isotopes*

The carbon, sulfur, and oxygen isotope study presented in this article points to several possible sources for the mineralizing fluids of Igarapé Bahia. However, a clear discrimination between these fluid sources that would support unequivocally a syngenetic or epigenetic model for Igarapé Bahia could not be attained.

The $\delta^{13}C$ results (from −6.7 to −13.4 per mil) for carbonates, for instance, indicate that carbon derives from deep-seated, possibly magmatic, and organic sources, whereas the $\delta^{18}O$ signatures from carbonates (from 4.7 to 20.7 per mil) point to a $\delta^{18}O$-rich, magmatic or sedimentary source. Compared to other deposits and reservoirs, the Igarapé Bahia carbonates are distinctly lighter than marine carbonates, which have $\delta^{13}C$ values of −5 to 5 per mil (Rollinson 1995: see field 3, Fig. 8a), and carbonates associated with VHMS deposits, which usually have $\delta^{13}C$ values between −5 and 2 per mil (Huston 1999: field 1, Fig. 8a). They also differ from the Olympic Dam siderites, which have $\delta^{13}C$ values from −2.4 to 3.5 per mil (Oreskes and Einaudi 1992: field 2, Fig. 8a).

The $\delta^{34}S$ isotopic results, from −1.1 to 5.6 per mil, with an outlier at −10.8 per mil, indicate that most sulfur in chalcopyrite is magmatic or leached from magmatic rocks, whereas some contribution of reduced and oxydized sulfur is also present. The concentration of $\delta^{34}S$ values around 0 per mil is consistent with the variation presented by Archean VHMS deposits, characterized by sulfide $\delta^{34}S$ values of 1±1 per mil (Ohmoto and Goldhaber 1997), and this is also suggested by Villas et al. (2001) and Dreher (2004). However, most IOCG deposits have $\delta^{34}S$ values in the 0± 5 per mil range (Williams et al. 2005) so that a distinction between these deposit types based on $\delta^{34}S$ data is difficult.

The $\delta^{18}O$ composition calculated for the ore fluids (from 5 to 16.5 per mil) suggests a magmatic input and/or interaction with $\delta^{18}O$-rich, possibly sedimentary rocks. This range in $\delta^{18}O_{fluid}$ is not common in volcanogenic sulfide deposits, which normally have $\delta^{18}O$ fluid compositions between −2 and 4 per mil (Huston 1999, see Fig. 10), indicating that the mineralizing fluids are essentially derived from seawater ($\delta^{18}O \cong 0$ per mil). However, the involvement of anomalous, $\delta^{18}O$-rich fluids has been reported in the case of some VHMS deposits. Examples include the Archean Kidd Creek deposit in Canada, with $\delta^{18}O_{fluid}$ values from 6 to 9 per mil (Beaty and Taylor 1982; Beaty et al. 1988, see Fig. 10) and the Triassic Besshi-type Windy Craggy deposit, also in Canada, with $\delta^{18}O_{fluid}$ of 0 to 14 per mil (Peter and Scott 1999, Fig. 10). The $^{18}O$ enrichment in these deposits is attributed either to fluids that underwent evaporation or interaction with sedimentary rocks, or, alternatively, to the addition of magmatic brines to the hydrothermal systems. The ranges of $\delta^{18}O_{fluid}$ compositions for the Olympic Dam

deposit and for many other Australian IOCG deposits are provided in Fig. 10. The $\delta^{18}O_{fluid}$ values for the Olympic Dam deposit range from −2.5 to 10 per mil (Oreskes and Einaudi 1992) and are explained by mixing of at least two fluids, one $\delta^{18}O$-enriched, of magmatic or deeply-circulated meteoric origin, and the other, of lower $\delta^{18}O$ values, of meteoric and oxidized nature (Haynes et al. 1995). Other Australian Proterozoic IOCG deposits (Fig. 10) commonly have $\delta^{18}O_{fluid}$ compositions from around 7 to 13 per mil, for which magmatic and/or metamorphic fluid contributions have been suggested, but according to Williams et al. (2005), this appears to be largely consistent with rock equilibration.

Recent boron isotopic analyses on tourmalines of Igarapé Bahia (Xavier et al. 2005) provide an unambiguous evidence with regard to potential hydrothermal fluid sources. The analyzed tourmalines occur disseminated in the ore-bearing breccia matrix and display very heavy $\delta^{11}B$ compositions, from 12 to 26 per mil, that are typical of a marine evaporitic boron source (Palmer and Swihart 1996). These data indicate an evaporitic source for the highly saline mineralizing fluids of Igarapé Bahia.

The presence of evaporites in the Carajás region has not been demonstrated yet. However there are many scapolite-bearing rocks in the volcano-sedimentary units of the Itacaiúnas Supergroup which could represent meta-evaporites, such as, for example, the biotite–tourmaline–scapolite–schists described from the Sossego deposit area by Villas et al. (2005).

Concerning evaporitic fluids, Barton and Johnson (1996, 2000) point out that these fluids cannot only mobilize large quantities of metals by Cl-complexing but can also exert a control upon the ore paragenesis in related mineral deposits. Evaporite-derived brines tend to have a high oxidation state and to be rich in $Ca^{2+}$ and sulfate from dissolution of gypsum, which will keep the dissolved reduced sulfur quite low (McKibben and Hardie 1997). Consequently, these fluids preferentially precipitate oxides—like magnetite or hematite—carbonates, phosphates, and silicates. Copper sulfides are formed preferentially because copper is the least soluble chalcophile element while Pb and Zn remain in solution.

Thus, an evaporitic source as suggested by the B isotope composition of tourmaline may explain the generation of the highly saline fluids for the hydrothermal system of Igarapé Bahia as well as the oxidized paragenesis of the deposit. This explanation excludes a significant participation of granitic or mantle-derived fluids, reinforcing the role of nonmagmatic brines in the genesis of the fragmental rock-hosted ore of Igarapé Bahia.

*Hydrothermal fluids and isotopes in the late veins*

The quartz–calcite–chalcopyrite veins that cut all rocks in the Igarapé Bahia deposit area indicate later mineralization events at Igarapé Bahia. However, fluid inclusion data on these veins show that they formed from saline-aqueous (up to 40 wt% salinity), chemically complex ($NaCl–CaCl_2–H_2O±FeCl_2$) fluids that, except for the rare presence of $CO_2$, were similar to the fluids that percolated through the fragmental rock unit. The $\delta^{13}C$ and $\delta^{34}S$ isotope values of the vein carbonates and chalcopyrites, respectively, are also similar to those obtained for the same minerals in the fragmental rock and may indicate similar carbon and sulfur sources. The main difference lies in a meteoric component in the mineralizing fluids of the veins ($\delta^{18}O$ ~0 per mil) not detected in the fragmental rock fluids.

Yardley (2005) points out that repeated episodes of base metal mineralization in the same area may reflect the continued presence of chloride in the rock column, either in the form of brines or evaporite strata. These Cl-rich fluids or rocks have long residence times and are only slowly removed or dissolved. Thus, it is possible that mineralization associated with the late veins may be the result of later hydrothermal events in the Igarapé Bahia area that involved circulation of saline fluids derived from the same evaporite beds or ancient brines that acted as sources for the fluids that mineralized the fragmental rock unit.

## Conclusions

1. Considering the geological setting, the Igarapé Bahia fragmental rock-hosted Cu–Au deposit has several features in common with syngenetic deposits. These include the volcano-sedimentary context, the strata-bound character of the deposit, and its association with submarine basaltic flows, hyaloclastite, and exhalative beds such as BIF and chert. However, reliable age determinations are not available to attest that mineralization was contemporaneous with host rock formation at 2,750 Ma.
2. Other geological evidence, such as the foliated structure of most fragmental rocks, implying formation before deformation, and the confinement of the fragmental unit to the Itacaiúnas host rocks without transecting the Águas Claras meta-arenites that cover part of the orebodies, also indicate that the deposit could be coeval with, or close in age to, the host sequence. In this context, the 2,575-Ma U–Pb monazite age (Tallarico et al. 2005) could probably represent a later, superimposed event and not necessarily the main mineralization episode at Igarapé Bahia. Additionally, because granites, such as the Old Salobo granite, are small and poorly represented in the Carajás Province, the correlation of granite magmatism and the Igarapé Bahia mineralization is doubtful.
3. Considering the highly saline mineralizing fluids, with up to 45 wt% salinity, and the distinct ore mineral

assemblage, dominated by chalcopyrite and magnetite, with gold, U- and LREE-minerals and scarce pyrite, Igarapé Bahia belongs to the Fe oxide Cu–Au (IOCG) group of deposits.

4. The C, S, and O isotope data obtained in this study do not clearly discriminate between fluid sources. However, B isotope data obtained on tourmaline (Xavier et al. 2005) provide strong evidence of the involvement of a marine evaporitic source in the mineralizing fluids of Igarapé Bahia. Evaporite-derived fluids may explain the high salinity and the relatively oxic mineral paragenesis dominated by chalcopyrite and magnetite. An evaporitic source may also explain repeated mineralization episodes in the same area (Yardley 2005). The quartz–chalcopyrite–calcite veins that cut all rocks of the Igarapé Bahia deposit area may represent such episodes, as they were also formed from very saline fluids and from apparently similar carbon and sulfur sources as those that generated the fragmental rock mineralization.
5. Although displaying attributes of an IOCG deposit with regards to the mineralizing fluids and metal paragenesis, Igarapé Bahia exhibits geological characteristics that suggest a syngenetic formation. As the mineralizing fluids were dominantly nonmagmatic, there exists the possibility that the deposit was generated by a hydrothermal submarine system whose elevated salinity was acquired by leaching of evaporite beds. However, this possibility remains to be proved or discarded, depending upon future research effort at the Igarapé Bahia deposit.

**Acknowledgments** This research was funded by CPRM-Geological Survey of Brazil, FAPESP-Fundação de Amparo à Pesquisa no Estado de São Paulo (Pr. 99/03058), and CAPES-Coordenação do Pessoal de Nível Superior (Pr. BEX0885/01-0). Field work at Carajás was made possible by the support of CVRD-Companhia Vale do Rio Doce. Many geologists at the Igarapé Bahia mine, in particular J.L. Rego, H. Meireles, A. Nunes and B. Aires, are thanked for important information and guidance besides providing geological maps, sections, and access to drill core. D. Silva is thanked for assistance during fluid inclusion, Raman microspectroscopy, and electron microscope studies carried out at UNICAMP-University of Campinas. M.Z. Moreira and H. Mirnejad are thanked for the isotopic analyses carried out at CENA-Centro de Energia Nuclear na Agricultura, in Piracicaba, Brazil, and at the Light Stable Isotope Laboratory of the Geological Survey of Canada, in Ottawa, respectively. This paper has benefited greatly from comments and suggestions by D.I. Groves and an anonymous reviewer. The paper also benefited from thorough reviews by S. Hagemann and B. Lehmann. Their careful reading and suggestions on early versions of this article helped to improve it significantly.

## References

Al-Assam IS, Taylor BE, South BS (1990) Stable isotope analysis of multiple carbonate samples using selective acid extraction. Isot Geosci 80:119–125

Almada MCO, Villas RNN (1999) O depósito Bahia: um possível exemplo de depósito vulcanogênico tipo Besshi arqueano em Carajás. Rev Bras Geociênc 29:579–592

Anderson MR, Rankin AH, Spiro B (1992) Fluid mixing in the generation of mesothermal gold mineralization in the Transvaal Sequence, Transvaal, South Africa. Eur J Mineral 4:933–948

Ayers JC, Loflin M, Miller CF, Barton MD, Coath C (2004) Dating fluid infiltration using monazite. In: Wanty RB, Seal II RR (eds) Proceedings of the Eleventh International Symposium on Water-Rock Interaction, 1:247–251. Balkema Publishers

Barreira CF, Soares ADV, Ronzé PC (1999) Descoberta do depósito Cu–Au Alemão—Província Mineral de Carajás (PA). In: SBG, 6° Simpósio de Geologia da Amazônia, Manaus, AM. Bol Res Expandidos, pp 136–139

Barros CEM, Dall'Agnol R, Lafon JM, Teixeira NP, Ribeiro JW (1992) Geologia e geocronologia Rb-Sr do gnaisse Estrela, Curionópolis, PA. Bol Mus Para Emílio Goeldi 4:83–102

Barros CEM, Macambira MJB, Barbey P (2001) Idade de zircão do Complexo Granítico Estrela: relações entre magmatismo, deformação e metamorfismo na Província Metalogenética de Carajás. In: SBG, 7° Simpósio de Geologia da Amazônia, Belém, PA. Resumos expandidos, CD-ROM

Barros CEM, Macambira MJB, Barbey P, Scheller T (2004) Dados isotópicos Pb-Pb em zircão (evaporação) e Sm-Nd do Complexo Granítico Estrela, Província Mineral de Carajás, Brasil: implicações petrológicas e tectônicas. Rev Bras Geociênc 34:531–538

Barton MD, Johnson DA (1996) Evaporitic-source model for igneous-related Fe-oxide-(REE-Cu–Au-U) mineralization. Geology 24:259–262

Barton MD, Johnson DA (2000) Alternative brine sources for Fe-oxide (-Cu–Au) systems: implications for hydrothermal alteration and metals. In: Porter TM (ed) Hydrothermal iron oxide copper-gold & related deposits: a global perspective. Australian Mineral Foundation, Adelaide, pp 43–60

Beaty DW, Taylor HP (1982) Some petrologic and oxygen isotopic relationships in the Amulet Mine, Noranda, Quebec, and their bearing on the origin of Archean massive sulfide deposits. Econ Geol 77:95–108

Beaty DW, Taylor HP, Coad PR (1988) An oxygen isotope study of the Kidd Creek, Ontario, volcanogenic massive sulfide deposit: evidence for a high $^{18}O$ ore fluid. Econ Geol 83:1–17

Beaudoin G, Taylor BE (1994) High precision and spatial resolution sulfur isotope analysis using MILES laser microprobe. Geochim Cosmochim Acta 58:5055–5063

Bodnar RJ (1993) Revised equation and table for determining the freezing point depression of $H_2O$-NaCl solutions. Geochim Cosmochim Acta 57:683–684

Bodnar RJ (2003) Introduction to aqueous-electrolyte fluid inclusions. In: Samson I, Anderson A, Marshall D (eds). Fluid Inclusions: analysis and interpretation. Mineralogical Association of Canada. Short Course Ser 32:81–100

Bottinga Y, Javoy M (1973) Comments on oxygen isotope geothermometry. Earth Planet Sci Lett 20:250–265

Bouma AH (1962) Sedimentology of some flysch deposits. Elsevier, Amsterdam, p 162

Chen HS (1972) The thermodynamics and composition of carbon dioxide hydrate. MSc.Thesis, Syracuse University, New York, p 86

Clayton RN, Mayeda TK (1963) The use of bromine pentafluoride in the extraction of oxygen from oxides and silicates for isotopic analysis. Geochim Cosmochim Acta 27:43–52

Cordeiro A (1999) Pesquisa mineral: panorama atual da CVRD na Amazônia. In: SBG, 6° Simpósio de Geologia da Amazônia, Manaus, AM. Bol Res Expandidos, pp 80–83

Daleffe DL (2001) Brechas mineralizadas: parâmetros de classificação e aplicação ao depósito de Cu–Au de Igarapé Bahia, Província

Mineral de Carajás, PA. Relatório Final de Iniciação Científica. IG-UNICAMP, Campinas, SP. p 16

Dardenne MA, Ferreira Filho CF, Meirelles MR (1988) The role of shoshonitic and calc-alkaline suites in the tectonic evolution of the Carajás District, Brazil. J South Am Earth Sci 1:363–372

Davis DW, Schandl ES, Wasteneys HA (1994) U-Pb dating of minerals in alteration halos of Superior Province massive sulfide deposits: syngenesis versus metamorphism. Contrib Mineral Petrol 111:427–437

Dias GS, Macambira M.B, Dall'Agnol R, Soares ADV, Barros CEM (1996) Datação de zircão de sill de metagabro: comprovação da idade arqueana da Formação Águas Claras, Carajás, Pará. In: SBG, 5° Simpósio de Geologia da Amazônia, Belém, PA, Bol Res Expandidos, pp 376–379

Docegeo (1988) Revisão litoestratigráfica da Província Mineral de Carajás. In: SBG, 35° Congresso Brasileiro de Geologia, Belém, PA, Anexo dos Anais, Província Mineral de Carajás—Litoestratigrafia e principais depósitos minerais, p 165

Dreher AM (2004) O depósito primário de Cu–Au de Igarapé Bahia, Carajás: rochas fragmentárias, fluidos mineralizantes e modelo metalogenético. Tese de Doutorado, Unicamp, Campinas, SP, p 221

Dreher AM, Xavier RP (2001) Provável origem e processo de mineralização das brechas do depósito de Igarapé Bahia, Carajás. In: SBG, 7° Simpósio de Geologia da Amazônia, Belém, PA. Resumos Expandidos, CD-ROM

Dreher AM, Xavier RP, Martini SL (2005) Fragmental rocks of the Igarapé Bahia Cu–Au deposit, Carajás Mineral Province, Brazil. Rev Bras Geociênc 35:359–368

Einsele G (1991) Submarine mass flow deposits and turbidites. In: Einsele G, Ricken W, Seilacher R (eds) Cycles and events in stratigraphy. Springer, Berlin Heidelberg New York, pp 313–339

Evans AM (1995) Introduction to mineral exploration. Blackwell, Oxford, p 396

Ferreira Filho CF (1985) Geologia e mineralizações sulfetadas do prospecto Bahia, Província Mineral de Carajás. Universidade de Brasília, DF, Tese de Mestrado, p 112

Franklin JM (1993) Volcanic-associated massive sulphide deposits. In: Kirkham RV, Sinclair WD, Thorpe RI, Duke JM (eds) Mineral deposit modelling, Geological Association of Canada, Special Paper 40, pp 315–334

Friedman I, O'Neil JR (1977) Compilation of stable isotope fractionation factors of geochemical interest. In: Fleischer M (ed) Data of geochemistry. Sixth edn. US Geological Survey Professional Paper 440-KK:1–12

Galarza MA (2002) Geocronologia e geoquímica isotópica dos depósitos de Cu–Au Igarapé Bahia e Gameleira, Província Mineral Carajás (PA), Brasil. Tese de Doutorado, Universidade Federal do Pará, p 214

Galarza MA, Macambira MJB (2002) Petrologia e geocronologia das rochas encaixantes do depósito de Cu–Au Igarapé Bahia, Província Mineral de Carajás, Pará, Brasil. In: Klein EL, Vasquez ML, Rosa-Costa LT (eds) Contribuições à Geologia da Amazônia 3:153–168

Galarza MA, Macambira MJB, Villas RN (2006) Age and isotopic characteristics (Pb and S) of the Fe Oxide-Cu-Au-U-REE Igarapé Bahia ore deposit, Carajás Mineral Province, Pará State, Brazil. In: Dall'Agnol R, Rosa-Costa LT, Klein EL (eds) Symposium on magmatism, crustal evolution, and metallogenesis of the Amazonian Craton. PRONEX-UFPA/SBG-NO, Belém, PA. Abstract Volume and Field Trips Guide, pp 19

Gibbs AK, Wirth KR, Hirata WK, Olszewski WJ Jr (1986) Age and composition of the Grão Pará Group volcanics, Serra dos Carajás. Rev Bras Geociênc 16:201–211

Groves DI, Vielreicher NM (2001) The Phalabowra (Palabora) carbonatite-hosted magnetite-copper sulfide deposit, South Africa: an end-member of the iron oxide copper-gold-rare earth element group? Miner Depos 36:189–194

Haynes DW, Cross KC, Bills RT, Reed MH (1995) Olympic Dam ore genesis: a fluid mixing model. Econ Geol 90:281–307

Hitzman MW, Oreskes N, Einaudi M (1992) Geological characteristics and tectonic setting of Proterozoic iron-oxide (Cu, U, Au, REE) deposits. Precambrian Res 58:241–287

Hoefs J (1987) Stable isotope geochemistry. Springer, Berlin Heidelberg New York, p 241

Holdsworth RE, Pinheiro RVL (2000) The anatomy of shallow-crustal transpressional structures: insights from the Archean Carajás fault zone, Amazon, Brazil. J Struct Geol 22:1105–1123

Huhn SB, Nascimento JAS (1997) São os depósitos cupríferos de Carajás do tipo Cu–Au-U-ETR? In: Costa ML, Angélica RS (eds) Contribuições à Geologia da Amazônia. SBG, Belém, pp 143–160

Huston DL (1999) Stable isotopes and their significance for understanding the genesis of volcanic-hosted massive sulfide deposits: a review. In: Barrie CT, Hannington MD (eds) Volcanic-associated massive sulfide deposits: processes and examples in modern and ancient settings. Rev Econ Geol 8:157–179

Kerrich R (1990) Carbon isotope systematics of Archean Au-Ag vein deposits in the Superior Province. Can J Earth Sci 27:40–56

Klein C (1973) Changes in mineral assemblages with metamorphism of some banded Precambrian iron-formation. Econ Geol 68:1075–1088

Laux JH, Lindenmayer ZG, Santos TR (2003) Características gerais dos depósitos do tipo óxido de ferro (Cu-U-Au-ETR): o exemplo da Província Mineral de Carajás. In: Ronchi JH, Althoff FJ (org) Caracterização e modelamento de depósitos minerais. Editora Unisinos-Capes, São Leopoldo, RS, pp 41–68

Lindenmayer ZG, Fyfe WS (1992) Comparação preliminar entre os metabasaltos dos grupos Parauapebas e Salobo da Bacia Carajás, Estado do Pará. In: SBG, 37° Congresso Brasileiro de Geologia, Resumos Expandidos 2:33–34

Lindenmayer ZG, Laux JH, Teixeira JBG (2001) Considerações sobre a origem das formações ferrífera da Formação Carajás, Serra dos Carajás. Rev Bras Geociênc 31:21–28

Lowe DR (1975) Water escape structures in coarse-grained sediments. Sedimentology 22:157–204

Macambira JB (1992) Os possíveis microfósseis na Formação Carajás. In: Sociedade Brasileira de Geologia, Congresso Brasileiro de Geologia 37, São Paulo, SP, Resumos 1:483–484

Machado N, Lindenmayer ZG, Krogh E, Lindenmayer D (1991) U-Pb geochronology of Archean magmatism and basement reactivation in the Carajás area, Amazon Shield, Brazil. Precambrian Res 49:329–354

Matsuhisa Y, Goldsmith JR, Clayton RN (1979) Oxygen isotopic fractionation in the system quartz-albite-anorthite-water. Geochim Cosmochim Acta 43:1131–1140

McCrea M (1950) The isotopic chemistry of carbonates and a paleotemperature scale. J Chem Phys 18:849–857

McKibben MA, Hardie LA (1997) Ore-forming brines in active continental rifts. In: Barnes HL (ed) Geochemistry of hydrothermal ore deposits, 3rd edn. Wiley, New York, pp 877–935

McPhie J, Doyle M, Allen R (1993) Volcanic textures: a guide to the interpretation of textures in volcanic rocks. University of Tasmania, CODES, p 198

Ohmoto H, Goldhaber MB (1997) Sulfur and Carbon isotopes. In: Barnes HL (ed) Geochemistry of hydrothermal ore deposits, 3rd edn. Wiley, New York, pp 517–612

Olszewski WJ, Wirth KR, Gibbs AK, Gaudette HE (1989) The age, origin, and tectonics of the Grão Pará Group and associated rocks, Serra dos Carajás, Brazil: Archean continental volcanism and rifting. Precambrian Res 42:229–254

Oreskes N, Einaudi MT (1992) Origin of hydrothermal fluids at Olympic Dam: preliminary results from fluid inclusions and stable isotopes. Econ Geol 87:64–90

Palmer MR, Swihart GH (1996) Boron isotope geochemistry: an overview. In: Grew ES, Anovitz LM (eds) Boron mineralogy, petrology and geochemistry. Mineralogical Society of America. Rev Miner 33:709–744

Peter JM, Scott SD (1999) Windy Craggy, Northwestern British Columbia: the world's largest Besshi-type deposit. In: Barrie CT, Hannington MD (eds) Volcanic-associated massive sulfide deposits: processes and examples in modern and ancient settings. Rev Econ Geol 8:261–295

Pollard P (2006) An intrusion-related origin for Cu–Au mineralization in iron oxide–copper–gold (IOCG) provinces. Miner Depos 41:179–187

Ramboz C, Pichavant M, Weisbrod A (1982) Fluid immiscibility in natural processes: use and misuse of fluid inclusion data. II. Interpretation of fluid inclusion data in terms of immiscibility. Chem Geol 37:29–48

Réquia K, Fontboté L (2000) The Salobo iron oxide copper-gold ddeposit, Carajás, northern Brazil. In: Porter TM (ed) Hydrothermal iron oxide copper-gold & related deposits: a global perspective. Australian Mineral Foundation, Adelaide, South Australia, pp 225–236

Roedder E (1984) Fluid inclusions. Mineralogical Society of America. Rev Miner 12:644

Rollinson HR (1995) Using geochemical data: evaluation, presentation, interpretation. Longmans, England, p 352

Ronzé PC, Soares ADV, Santos MGS, Barreira CF (2000) Alemão copper-gold (U-REE) deposit, Carajás, Brazil. In: Porter TM (ed) Hydrothermal iron oxide copper-gold & related deposits: a global perspective. Australian Mineral Foundation, Adelaide, pp 191–202

Sangster DF (1999) Volcanic-exhalative massive sulphidde deposits. In: Silva MG, Misi A (eds) Base metal deposits of Brazil. MME-DNPM-CPRM, Belo Horizonte, pp 33–43

Santos MGS (2002) Estudo dos isótopos de Pb e Nd do depósito de Cu–Au (U-ETR) Alemão, Província Mineral de Carajás (PA). Universidade Federal do Pará, Belém, PA, Tese de Mestrado, p. 121

Schandl ES, Gorton MP (1991) Postore REE mobility at Kidd Creek and at other Archean massive sulfide deposits. Econ Geol 86:1446–1553

Shepherd TJ, Rankin AH, Alderton DHM (1985) A practical guide to fluid inclusion studies. Blackie, Glasgow p 239

Sterner SM, Hall DL, Bodnar RJ (1988) Synthetic fluid inclusions V: solubility relations in the system NaCl-KCl-$H_2O$ under vapor-saturated conditions. Geochim Cosmochim Acta 52:989–1005

Tallarico FHB, McNaughton NJ, Groves DI, Fletcher IR, Figueiredo BR, Carvalho JB, Rego JL, Nunes AR (2004) Geological and shrimp II U-Pb constraints on the age and origin of the Breves Cu–Au-(W-Bi-Sn) deposit, Carajás, Brazil. Miner Depos 39:68–86

Tallarico FHB, Figueiredo BR, Groves DI, Kositcin N, McNaughton NJ, Fletcher IR, Rego JL (2005) Geology and Shrimp U-Pb geochronology of the Igarapé Bahia deposit, Carajás Copper-Gold belt, Brazil: an Archean (2.57 Ga) example of iron-oxide Cu–Au-(U-REE) mineralization. Econ Geol 100:7–28

Taylor BE (1986) Magmatic volatiles: isotopic variation of C,H, and S. Rev Miner 16:185–225

Taylor BE, Beaudoin G (1993) MILES laser microprobe. Part 1: system description. In: Current Research, Part D. Geological Survey of Canada, Paper 93-ID:191–198

Tazava E (1999) Mineralização de Au-Cu-(±ETR-U) associada às brechas hidrotermais do depósito de Igarapé Bahia, Província Mineral de Carajás, PA. Universidade Federal de Ouro Preto, MG, Dissertação de Mestrado, p 81

Tazava E, Oliveira CG (2000) The Igarapé Bahia Au-Cu-(REE-U) deposit, Carajás, Brazil. In: Porter TM (ed) Hydrothermal iron oxide copper-gold & related deposits: a global perspective. Australian Mineral Foundation, Adelaide, pp 203–212

Teixeira JBG, Eggler DH (1994) Petrology, geochemistry, and tectonic setting of Archean basaltic and dioritic rocks from the N4 iron ore deposit, Serra dos Carajás, Brazil. Acta Geol Leopold 40:71–114

Trendall AF, Basei MAS, Laeter JR, Nelson DR (1998) Shrimp zircon U-Pb constraints on the age of the Carajás formation, Grão Pará Group, Amazon Craton. J South Am Earth Sci 11:265–277

Villas RNN, Santos MD (2001) Gold deposits of the Carajás Mineral Province: deposit types and metallogenesis. Miner Depos 36:300–331

Villas RNN, Galarza MAT, Almada MCO, Viana AS, Ronzé PC (2001) Geologia do depósito Igarapé Bahia/Alemão, Província Carajás, Pará. In: Jost H, Brod JA, Queiroz ET (eds) Caracterização de depósitos auríferos em distritos mineiros brasileiros, DNPM/ADIMB, Brasília, DF, pp 215–240

Villas RN, Lima LFO, Neves MP, Sousa FDS, Lamarão CN, Fanton JJ, Morais R (2005) Relações entre deformação, alteração hidrotermal e mineralização no depósito de Cu–Au do Sossego, Província mineral de Carajás. In: I Simpósio Brasileiro de Metalogenia, Gramado, RS. Extended abstracts, CD-ROM

Williams PJ, Barton MD, Johnson DA, Fontboté L, Haller A, Mark G, Oliver NHS (2005) Iron oxide copper-gold deposits: geology, space-time distribution, and possible modes of origin. Econ Geol 100th Anniversary Volume, pp 371–405

Williams-Jones A, Samson IM (1990) Theoretical estimation of halite solubility in the system NaCl-$CaCl_2$-$H_2O$: applications to fluid inclusions. Can Mineral 28:299–304

Winter CJ (1994) Geology and base-metal mineralization associated with Archean iron-formation in the Pojuca Corpo Quatro deposit, Carajás, Brazil. University of Southampton, UK, Ph.D. thesis, p 300

Xavier RP, Wiedenbeck M, Dreher AM, Rhede D, Monteiro L, Araújo CEG (2005) Chemical and boron isotopic composition of tourmaline from Archean and Paleoproterozoic Cu–Au deposits in the Carajás Mineral Province. 1° Simpósio Brasileiro de Metalogenia, Gramado, Brazil, extended abstracts, CD-ROM

Yardley BWD (2005) Metal concentrations in crustal fluids and their relationship to ore formation. Econ Geol 100:613–632

Zang W, Fyfe WS (1995) Chloritization of the hydrothermally altered bedrock at the Igarapé Bahia gold deposit, Carajás, Brazil. Miner Depos 30:30–38

Zheng YF (1999) Oxygen isotope fractionation in carbonate and sulfate minerals. Geochem J 33:109–126